



Efficient removal of tizanidine and tetracycline from water: A single and competitive sorption approach using carboxymethyl cellulose granulated iron-pillared clay

Hanieh Khoshsima Bazkiaee^a, Seyedmehdi Sharifian^b, Neda Asasian-Kolur^{c,*}, Hanieh Najafi^a, Azadeh Ebrahimian Pirbazari^a, Michael Harasek^c

^a Fouman Faculty of Engineering, College of Engineering, University of Tehran, P.O. Box 43515-1155, Fouman 43516-66456, Iran

^b Davidson School of Chemical Engineering, Purdue University, West Lafayette, IN 47907, USA

^c Technische Universität Wien, Institute of Chemical, Environmental and Bioscience Engineering, Getreidemarkt 9/166, Vienna A-1060, Austria

ARTICLE INFO

Keywords:

Fe-pillared montmorillonite
Wastewater treatment
Competitive adsorption
Desorption

ABSTRACT

This study deals with the development of a granulated Fe-pillared clay (Fe-PC) using carboxymethylcellulose (CMC) as a binder to present it as an innovative adsorbent for the individual and competitive adsorption of tetracycline (Tc) and tizanidine (Tz) from water. An optimum pH value of 7 was determined for both individual and multi-component adsorption. The optimal dosage of granulated Fe-PC was determined to be 1.5 g/L for Tz and 3 g/L for Tc, resulting in constant removal rates of 80 % for Tc and 90 % for Tz. Tizanidine showed a higher affinity for powdered or granulated Fe-PC compared to tetracycline, due to its smaller molecular size and increased amine functional groups. Consequently, Tz showed improved kinetic rates (initial pseudo-second order sorption rates of 170.79 and 25.62 mg/g.h for Tz and Tc, respectively) and equilibrium capacities (maximum monolayer adsorption capacity of granulated Fe-PC at room temperature over Tc and Tz, 54.89 mg/g and 66.40 mg/g). Granulation affected the kinetic rate for both adsorbates, albeit with a more pronounced effect for Tc. The adsorption of Tz was less sensitive to temperature changes, indicating a lower enthalpy change of adsorption (14.24 and 77.91 kJ/mol for Tz and Tc, respectively). HCl for Tc and NaCl for Tz were identified as optimal desorption eluents, confirming the involvement of cation exchange in Tz adsorption. Surface functional group analysis confirmed the proposed complexation mechanisms. Tz consistently showed a higher affinity for granular Fe-PC than Tc, especially at lower adsorbent dosages. This article provides a comprehensive insight into the characterization of the prepared adsorbents and their cyclic adsorption-desorption performance for Tc and Tz.

1. Introduction

The presence of pharmaceutical pollutants as emerging contaminants in aquatic systems has raised concerns about their potential hazards to living organisms. These contaminants are non-biodegradable and require a high concentration of soluble oxygen to decompose. Despite conventional wastewater treatment methods, they remain in the environment [1,2]. In this article, tizanidine and tetracycline are presented as examples of painkillers and broad-spectrum antibiotics, respectively, and their removal from the aqueous environment.

Tizanidine is a skeletal muscle relaxant used to relieve muscle tension and spasms caused by brain and spinal cord injuries [3]. Tetracyclines, on the other hand, are widely used antibiotics and serve as a model substance for many case studies. Prolonged exposure to sublethal

concentrations of antibiotics can lead to the development of antibiotic-resistant bacteria in aquatic ecosystems, which could exacerbate the problem of antibiotic resistance in humans and animals. Furthermore, tetracycline can disrupt the balance of microbial communities in the aquatic environment, making it an exemplary pharmaceutical pollutant that requires a thorough assessment of its environmental impact [4,5].

Fig. 1(a) and (b) show the molecular structures of tetracycline and tizanidine. Tizanidine contains type II and III amine groups, which are crucial for its pharmacological activities and interactions. Tetracycline, with its complex molecular structure comprising a linear four-ring structure, has a broad spectrum of activity against various types of bacteria, making it a widely used antibiotic. Therefore, tetracycline serves as a valuable model compound for the study of pharmaceutical

* Corresponding author.

<https://doi.org/10.1016/j.apsadv.2024.100600>

Received 28 November 2023; Received in revised form 12 March 2024; Accepted 5 April 2024

Available online 9 April 2024

2666-5239/© 2024 The Author(s). Published by Elsevier B.V. This is an open access article under the CC BY-NC-ND license (<http://creativecommons.org/licenses/by-nc-nd/4.0/>).

pollutants.

Several methods have been proposed for the removal of pharmaceutical contaminants from aqueous systems, including membrane separation, advanced oxidation processes and adsorption processes [6]. The adsorption process is the preferred removal method when an easy-to-use, cost-effective and efficient method of removing trace contaminants is required. In addition, this method offers great flexibility in incorporating innovations during the synthesis of adsorbents and their surface modification, transforming a general-purpose adsorbent into a highly selective one [7]. However, it can also have disadvantages, such as the production of contaminated solids. This disadvantage can be mitigated by the production of recyclable adsorbents that are regenerable and can be used in cyclic adsorption-desorption processes.

Tetracycline has attracted considerable research attention due to its potential hazard and the need to study its removal by adsorption. Numerous reports have investigated various adsorbents and modification methods for the removal of tetracycline and compared their maximum monolayer adsorption capacities (q_m). These adsorbents include magnetic chitosan ($q_m=211.21$ mg/g) [8], mushroom bran-based biochar ($q_m=17$ mg/g) [9], polymeric adsorbent based on rubber waste ($q_m=76.33$ mg/g) [10], N-self-doped hierarchical porous carbon adsorbent ($q_m=506.6$ mg/g) [11], ZnAl-layered double hydroxide biochar composite ($q_m=41.98$ mg/g) [12], alkali-activated biochar based on walnut shells ($q_m=607$ mg/g) [13], sulfur-doped magnetic carbon nanotubes ($q_m=116.27$ mg/g) [14], poly (dopamine)-modified glass microspheres as a self-floating adsorbent ($q_m=333.7$ mg/g) [15], vitamin C-modified crayfish shell biochar ($q_m=293.36$ mg/g) [16], $g\text{-C}_3\text{N}_4\text{-ZnO-BaTiO}_3$ nanocomposite ($q_m=218.59$ mg/g) [17] and so on.

Tizanidine, a newer pharmaceutical pollutant, has received less attention in research. Its smaller molecular size and its structure, which contains nitrogen, sulfur and chlorine, give it a higher density of functionalities compared to tetracycline. This unique structure makes tizanidine suitable for comparative studies with tetracycline to investigate different adsorption mechanisms.

Researchers are constantly looking for new adsorbents with high capacity, fast kinetics, mechanical stability and regenerability to improve the efficiency of adsorption processes [18–20]. A variety of adsorbents have been utilized for the adsorption of tetracycline, as indicated by the existing literature [21]. The study investigates the effectiveness of porous clay-based adsorbents as a cost-effective approach. It utilizes the inherent porous nature of natural clays or synthetic zeolites, which can be further enhanced by swelling. Pillaring is a modification technique that increases the permanent porosity of

clay. By using different pillaring agents, clays with different surface areas, basal spacing, pore sizes, volumes and acid contents can be produced [22,23].

Iron-pillared clays are a magnetic, cost-effective and environmentally friendly adsorbent with high permanent porosity. They offer the additional advantage that the saturated sorbent can be easily separated and collected from the treated solution. Yuan et al. successfully synthesized and characterized dealuminated iron-pillared montmorillonite with a meso-microporous structure, which exhibited the highest specific surface area of 215.7 m²/g and the largest porosity of 0.29 cm³/g [24].

In this study, we investigate the use of iron-pillared clays as magnetic adsorbents, which have the great advantage of allowing a simple collection process. This separation process can be further improved by using extruded shaped granular adsorbents [25,26]. Among the various binders, the use of an environmentally friendly, easily accessible and cost-effective material is preferred for the production of new and innovative adsorbents.

Various types of binders have been proposed for the granulation of pillared clays, such as a hydrophilic silicone-acrylic polymer for high shear wet granulation of inorganic-organic pillared clays [27], gluten as a viscoelastic inert binder obtained by leaching wheat dough for granulation of iron pillared montmorillonite [28], and biopolymers including alginate, chitosan, or a combination of both used to encapsulate powdered silica pillared clay [29,30]. It is suggested that the presence of binders not only determines the shape and size of the particles but also confers specific functionalities that may increase/decrease their affinity for certain species. Carboxymethylcellulose (CMC) is a versatile material that can serve as a dispersing, thickening and gelling agent (Fig. 1(c)). Several studies have reported the use of CMC as a binder for the granulation of various adsorbents, such as chitosan [31], graphene oxide [32], and metal oxides [33]. In others, CMC has been introduced as an adsorbent [34].

In this study, we investigate the potential of carboxymethylcellulose (CMC) as a binder for the granulation and modification of Fe-pillared clay. We evaluate the adsorption capacity of the granulated product for two types of pharmaceutical pollutants, tetracycline (Tc) and tizanidine (Tz). This modification makes it possible to increase the particle size and improve the mechanical stability of the adsorbent. We compare the performance of powdered and granular Fe-PC in the removal of Tc and Tz. A comprehensive series of adsorption and desorption experiments in batch mode were performed with the granular sorbent to investigate the influence of different operating parameters on the adsorption, desorption and regenerability of the adsorbent. Kinetic, equilibrium and thermodynamic parameters were estimated by

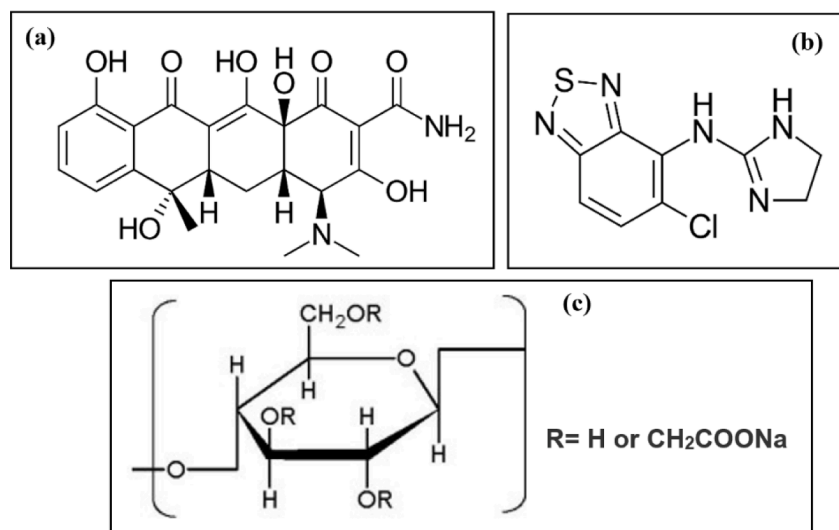


Fig. 1. Molecular structures of (a) tetracycline (Tc), (b) tizanidine (Tz) and (c) carboxymethylcellulose (CMC).

modeling and the mechanisms involved in adsorption were elucidated by a combination of characterization, adsorption and desorption studies. The most important innovations of the study are full-batch analysis of the adsorption behavior of tizanidine as a novel pharmaceutical pollutant, investigation of binary competitive adsorption of Tz and Tc, and the use of CMC-granulated Fe-pillared clay as a composite adsorbent for this application.

2. Experimental

2.1. Adsorbent preparation and granulation

In the current study, laboratory grade montmorillonite (Mt) (Sigma-Aldrich) was used to produce iron-pillared clay. Several chemicals were used for the preparation, including ferric nitrate nonahydrate ($\text{Fe}(\text{NO}_3)_3 \cdot 9\text{H}_2\text{O}$), sodium hydroxide (NaOH), carboxymethylcellulose ($\text{C}_8\text{H}_{16}\text{O}_8$), hydrochloric acid, ethanol ($\text{C}_2\text{H}_5\text{OH}$), sodium chloride (NaCl) and acetic acid (CH_3COOH) from Merck.

To ensure purity, the first step was to separate impurities such as minerals and carbonates from the montmorillonite. Mechanical sieving was carried out using sieve no. 325 and resulted in the separation and removal of particles larger than $45 \mu\text{m}$. The clay was then washed with distilled water (at a ratio of $10 \text{ mL}/1 \text{ mg Mt}$). The resulting Mt water was then separated by vacuum filtration and dried in an oven at 90°C .

To increase the purity, activity sites, porosity and acidity of the clay, an acid wash with acetic acid (0.25 M) was carried out at a ratio of $5 \text{ cm}^3/1 \text{ mg Mt}$. This treatment facilitated the removal of carbonate impurities, resulting in the production of CO_2 . After a 40-min wash with distilled water and vacuum filtration, the pretreated clay was dried in an oven at 90°C for 12 h.

The pretreated clay was then pulverized and subjected to NaCl treatment (1 M) for 14 h, which was repeated twice. The clay was then washed twice with distilled water for 1 h each time. The treated clay was finally dried in an oven at 90°C for 12 h.

Na-saturated clay was used for the production of iron-pillared clay. For this purpose, a pillaring solution was prepared by slowly adding a NaOH solution (0.2 M) to a $\text{Fe}(\text{NO}_3)_3$ solution (0.2 M) at a ratio of 1:2 with constant stirring on a magnetic stirrer for 1 h. This solution was

allowed to stand at 35°C for 24 h, then it was added dropwise to a 1% Na-saturated clay suspension and then stirred for another 24 h and vacuum filtered.

The treated clay was then subjected to several washing steps with distilled water (at a ratio of $1 \text{ g}/10 \text{ cm}^3$ for clay/water) over a period of 1 h, which was repeated four times. The washing process was continued until the pH of the filtrate reached that of distilled water. The clay was then dried in an oven at 85°C and subsequently pulverized. The product was calcined in the presence of air at 400°C for a total of 3 h. The result of this process was iron pillared clay represented by Fe-PC (as shown in Fig. 2).

Fig. 2 shows a schematic representation of the production of iron-pillared clay (Fe-PC) in conjunction with the granulation process using carboxymethylcellulose (CMC).

Carboxymethylcellulose (CMC) was used to granulate Fe-PC in a simple process. First, a CMC solution with a ratio of 1 to 50 (CMC to distilled water) was stirred for a period of 2 h at 45°C . In addition, an Fe-PC suspension was prepared at a ratio of 1 g to 10 cm^3 (clay to distilled water) for 2 h at room temperature. Both solutions were then combined and stirred for a further 4 h.

The resulting solution was then slowly added dropwise (with a 60 cm^3 syringe) to an $\text{Fe}(\text{NO}_3)_3$ (0.05 M) solution. On contact with the solution, the droplets turned into a granular form and cross-linking began. The resulting granules were left in the solution for 10 h before being washed three times with distilled water. Finally, the granulated hydrogels were dried at a temperature of 65°C . The resulting hydrogels and the dried granules are shown in Fig. 2.

2.2. Adsorbents' characterization

A number of analytical methods were used to characterize the raw materials and products in this study. The weight percentage of constituents contained in the clays and pillared clays was determined using X-ray fluorescence (XRF) analysis with a Rigaku spectrometer. The crystallinity and the phases present in the structures of the adsorbents were determined using an X-ray diffractometer (PHILIPS-PW1730) operated with an anode source of $\text{CuK}\alpha$ radiation ($\lambda=1.54056 \text{ \AA}$) at 40 kV and 30 mA. Fourier transform infrared spectroscopy (FTIR) was performed

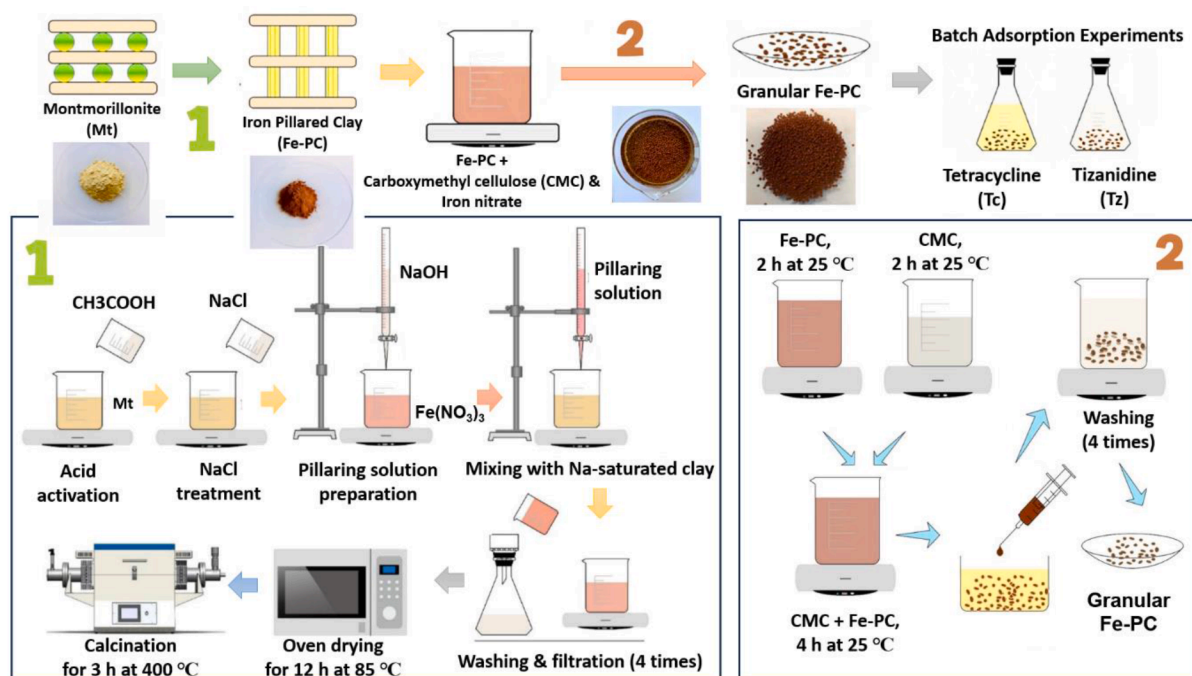


Fig. 2. A schematic representation of the preparation of iron-pillared clay (Fe-PC) (1) coupled with the granulation process using carboxymethylcellulose (CMC) (2).

using a Thermo AVATAR 360 and the spectra were measured in the 400–4000 cm^{-1} range. The aim of this analysis was to determine the functional groups and chemical bonds present in the products and other materials. The surface morphology of the adsorbents was analyzed using a TESCAN scanning electron microscope (FE-SEM). The specific surface area, pore size and micro- and mesopores of the adsorbents were determined using N_2 adsorption-desorption tests performed with a BELSORP mini II at 77 K. Diffuse reflectance spectroscopy (DRS) was performed in the 250–1100 nm range using an Avants-2048-TEC (DH-S Avants setup). The pH_{pzc} of the adsorbents was analyzed using a standard pH drift method. In this method, a 0.1 M NaCl solution was prepared and the pH of the solution was adjusted with 0.1 M NaOH and HCl in a range of 2–10. Adsorbents weighing 0.03 g were placed in contact with 30 cm^3 of the solutions for 20 h, and the pH of the solutions was determined after this time. The pH_{pzc} refers to the pH value at which the initial and final pH values are equal.

2.3. Single- and multi-component adsorption experiments

Solutions of tetracycline (Tc) and/or tizanidine (Tz) were prepared at initial concentrations of 30 mg/L to perform single-component adsorption experiments. The starting powders for tetracycline and tizanidine were provided by Tehrandarou Co, a local pharmaceutical manufacturing facility in Iran.

For the pH optimization experiments, 30 cm^3 of the Tc and Tz solutions (30 mg/L) were poured into 50 cm^3 Erlenmeyer flasks and the initial pH of each solution was adjusted with 0.1 M NaOH and HCl in the range of 3 to 11. Subsequently, 0.03 g of adsorbent was added to the solution, which was then shaken at room temperature (30 °C) at a speed of 250 rpm for 24 h. The effect of adsorbent dosage (from 0.2 to 3 g/L for tizanidine and from 0.1 to 4 g/L for tetracycline) was studied at an optimal pH of 7, while the other operating parameters were kept constant according to the pH experiments. Kinetic experiments were performed to determine the effect of contact time on adsorption, with contact times ranging from 5 min to 24 h for tizanidine and 5 min to 30 h for tetracycline. The experiments were continued until equilibrium was reached. Isothermal equilibrium adsorption tests were performed in the range of 10–300 mg/L for the initial concentration of pharmaceutical pollutants at three different temperatures (35, 45 and 55 °C).

In order to perform binary adsorption experiments, the adsorption of tetracycline and tizanidine was studied simultaneously at their individual initial concentrations of 30 mg/L. The influence of adsorbent dosage was studied in the range of 0.2–3 g/L, while the optimal pH for multicomponent adsorption was 7. The experiments were conducted under constant conditions, including a temperature of 30 °C, a shaking time of 24 h and a stirring speed of 250 rpm.

A UV–Vis spectrometer (Rayleigh UV-2601) was used to measure the concentrations of tizanidine and tetracycline. The maximum absorption wavelength for tizanidine and tetracycline was found to be 228 and 355 nm, respectively. Calibration of the device was performed over the concentration range of 10–30 mg/L for both Tz and Tc.

The agreement between the experimental data and the models was assessed using various statistical parameters. In addition to the R^2 (correlation coefficient), several other statistical parameters were used to assess the agreement between the kinetic and isotherm models (described in Sections 3.2.4 and 3.2.5) and the experimental data. The following equations are used to calculate SSE (Sum of Squared Errors) and RMSE (Root Mean Square Error):

$$SSE = \sum_i^n (q_{\text{exp}} - q_{\text{cal}})_i^2 \quad (1)$$

$$RMSE = \sqrt{\frac{\sum_i^n (q_{\text{exp}} - q_{\text{cal}})_i^2}{N}} \quad (2)$$

Where q_{cal} represents the calculated adsorption capacity, q_{exp} the

corresponding experimental value and N stands for the total number of data points. A value closer to 0 for these two parameters means that the model is better suited for predictive purposes.

2.4. Desorption experiments

The desorption experiments were carried out with sorbents that were completely saturated with either Tc or Tz. These experiments were performed following single-component equilibrium adsorption experiments that took place under optimal operating conditions, including a temperature of 30 °C, an initial concentration of 30 mg/L, a contact time of 24 h, a pH of 7, a shaking rate of 250 rpm, and an optimal adsorbent dosage of 3 g/L for Tc and 1.5 g/L for Tz. After primary adsorption, the saturated sorbents were separated from the treated solutions via filter paper. The solid samples were then dried for 4 h at a temperature of 70 °C and the filtrate was analyzed by UV–Vis spectroscopy.

Three different eluents, namely 0.1 M NaCl, 0.1 M HCl and ethanol, were used in the desorption experiments on the saturated sorbents. For the desorption process, an adsorbent dosage twice as high as the optimal adsorption dosage (6 g/L for Tc and 3 g/L for Tz) was used. From an economic and technical point of view, it is more favorable to desorb the adsorbed species in a smaller volume of the desorption solution and to obtain a more concentrated solution with a smaller volume. Therefore, we propose to halve the volume of the eluent instead of desorbing the species in a volume equal to that of the feed solution. This means that the solid dosage in the desorption process is twice as high as in the adsorption process.

The desorption experiments were carried out for 6 h at 30 °C with a shaking rate of 250 rpm. After the desorption experiments, the sorbents were separated from the eluents by filtration, rinsed, dried and then used for the next adsorption experiments. The adsorption-desorption and recovery experiments were performed cyclically with five consecutive cycles.

Each adsorption and desorption experiment was repeated twice, and the resulting error percentage was less than 5 %.

3. Results and discussion

3.1. Characterization studies

One of the most important results of the characterization confirming the incorporation of Fe and the replacement of other metals by Fe in the pillared and granular pillared clays, is shown in Table 1, which shows the XRF results. From the data, the Fe content in the raw montmorillonite before any treatment was about 6.5 wt%, which increased significantly to about 22 wt% after iron pillaring. The granulation process, which was carried out in an $\text{Fe}(\text{NO}_3)_3$ solution, further increased the Fe content to 26 wt%.

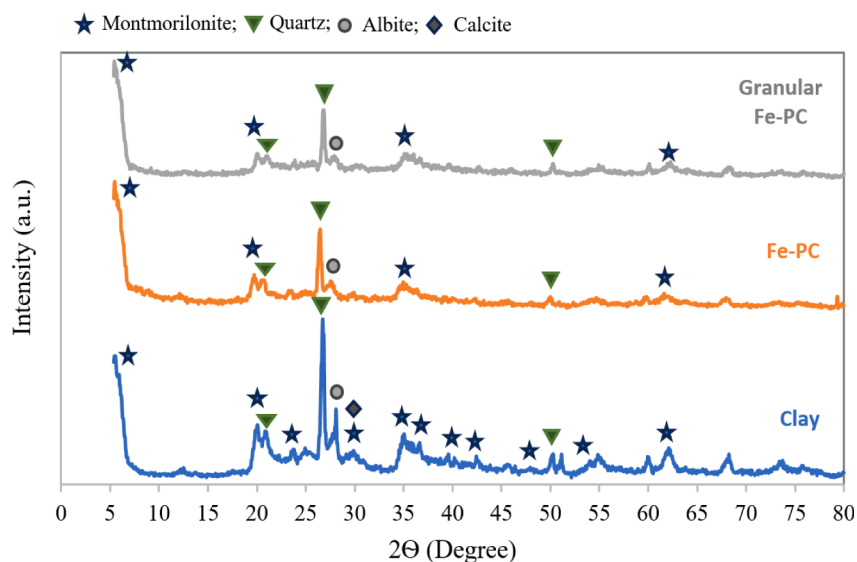
In addition, Table 1 shows the LOI% as an estimation of the presence of volatiles, including water, carbon dioxide and organic matter in the clay material. During the pillarization process, various purification and treatment steps were carried out, resulting in a decrease in LOI from about 13 % to about 10 %. However, after granulation with CMC and due to the addition of organic molecules from the binder, this parameter increased to over 26 %.

Fig. 3 shows the XRD patterns of three clay samples, which allow a comparison of their crystallinity and the identification of the phases within their structure. The raw clay pattern shows the characteristic peaks of montmorillonite (JCPDS Card No. 13–0135). The peak at $2\theta=5.49^\circ$, which represents the basal spacing (d001) of montmorillonite, was not significantly altered by Fe-pillarization or granulation. Typically, the basal spacing of the clay (both raw and modified) was estimated to be about 16 Å, suggesting that the $\text{Fe}(\text{NO}_3)_3$ -mediated pillarization process did not alter the interlayer spacing of the montmorillonite clay. Nevertheless, it played a role in the development and maintenance of constant porosity.

Table 1

Weight percentages of oxides and Loss on Ignition (LOI) in the structure of raw clay (montmorillonite), Fe-pillared clay, and granular Fe-pillared clay.

Sample	Weight percentage (% wt.) (excluding LOI)											LOI%
	SiO ₂	Al ₂ O ₃	Fe ₂ O ₃	CaO	MgO	K ₂ O	Na ₂ O	TiO ₂	SO ₃	P ₂ O ₅	MnO	
Mt (Clay)	63.97	20.72	6.49	2.13	2.01	1.68	1.37	0.77	0.53	0.23	0.10	12.99
Fe-PC	55.99	17.29	22.38	0.28	1.07	1.37	0.69	0.68	0.08	0.17	<	9.92
Granular Fe-PC	53.76	15.56	25.95	0.23	1.78	1.19	0.58	0.63	0.17	0.13	<	26.27

**Fig. 3.** XRD patterns of montmorillonite clay, iron pillared clay in the powdered and granular forms.

In addition, the raw clay contained quartz as an impurity, which had a highly crystalline structure and significantly affected the XRD pattern (JCPDS Card No. 46–0145). During the pre-treatment phases for pillaring and granulation, the presence of impurities such as quartz was reduced and/or masked by organic binders. Therefore, the intensity of the quartz peak was lower in the XRD patterns of Fe-PC and granulated Fe-PC.

Pillarization of raw clays is primarily aimed at increasing their porosity by introducing inner columns into the structure of the resulting pillared clays. In the present study, an attempt was made to investigate the effects of pillarization on the samples by performing N₂ adsorption-desorption experiments at 77 K. The resulting isotherms were classified according to the IUPAC classification scheme and are shown in Fig. 4(a) for further analysis.

All clay samples exhibited a type II adsorption isotherm, indicating a low proportion of micropores (due to the low amount of adsorbed N₂ at low partial pressures) and a higher proportion of mesopores due to the presence of a relatively large hysteresis loop at relatively high partial pressures. The hysteresis loops all belong to the H₄ classification, which is characterized by a slit-shaped pore morphology [35]. These results may provide insights into the potential applications of pillared clays, especially for mesoporous materials.

The porous properties of the clay samples were compared in Table 2 to show that pillarization increases the specific surface area of the clay sample by a factor of three. However, granulation of the Fe-PC with CMC slightly reduced this specific surface area from 114 m²/g to less than 100 m²/g. The total pore volume and mesopore volume of the samples followed a similar trend. The BJH mesopore width of the samples was calculated from the desorption data and ranged between 38.6 to 28.9 Å. The percentage of mesopore volume relative to the total pore volume of the samples was also calculated. The raw clay had a percentage of approximately 100 %, while the treated clays had a percentage of approximately 88–89 %. These results indicate that the process of

pillarization created and enlarged some micropores in the structure of the pillared clays.

The FESEM images in Fig. 4(b) clearly show the differences in the porous properties of the clay samples. As a non-porous material, the raw clay exhibited relatively low porosity, as can be seen in Fig. 4 (b-1). However, after pillarization, the clay samples showed discernible pores and an increase in porosity, especially in the mesoporous region, along with slit-shaped pores, as shown in Fig. 4 (b-1). It was observed that the addition of a CMC binder to the granulated sample covered the surface slits, resulting in a reduction in specific surface area, as shown in Fig. 4 (b-3).

The surface functionalities of the adsorbents were investigated and compared using FTIR analysis. The corresponding spectra are shown in Fig. 5. It is evident that the spectra of all three clay samples, including the raw montmorillonite, the Fe-PC and the granular pillared clay, have a similar shape. Table 3 gives an overview of the main peaks detected in the samples. The aim of the analysis was to identify any differences between the samples and to find evidence for the addition of new groups during the treatments. The OH stretching bonds associated with the hydroxyl elongation of the octahedral layer of the clay [36,37] were prominent in all three samples. However, at about 2920 cm⁻¹ and 1700 cm⁻¹ the granular Fe-PC shows small peaks that cannot be detected in the raw clay and Fe-PC. These small peaks can be attributed to the C–H stretching vibrations [38] and the aliphatic C = O and –COOH stretching vibrations [39], respectively, as indicated in Table 3. This suggests the possible introduction of CMC as an organic binder in the clay structure.

On the other hand, the analysis of the FTIR spectra does not indicate the inclusion of Fe in the Fe-PC structure compared to montmorillonite clay. In fact, the presence of Fe–O stretching vibrations and Fe–O–Fe bridging vibrations on the Fe-PC surface cannot be conclusively demonstrated due to overlap with other dominant groups [40]. A literature search shows that the peaks associated with Fe–O bonds typically fall in the range of 450 to 700 cm⁻¹ [41–44]. For example,

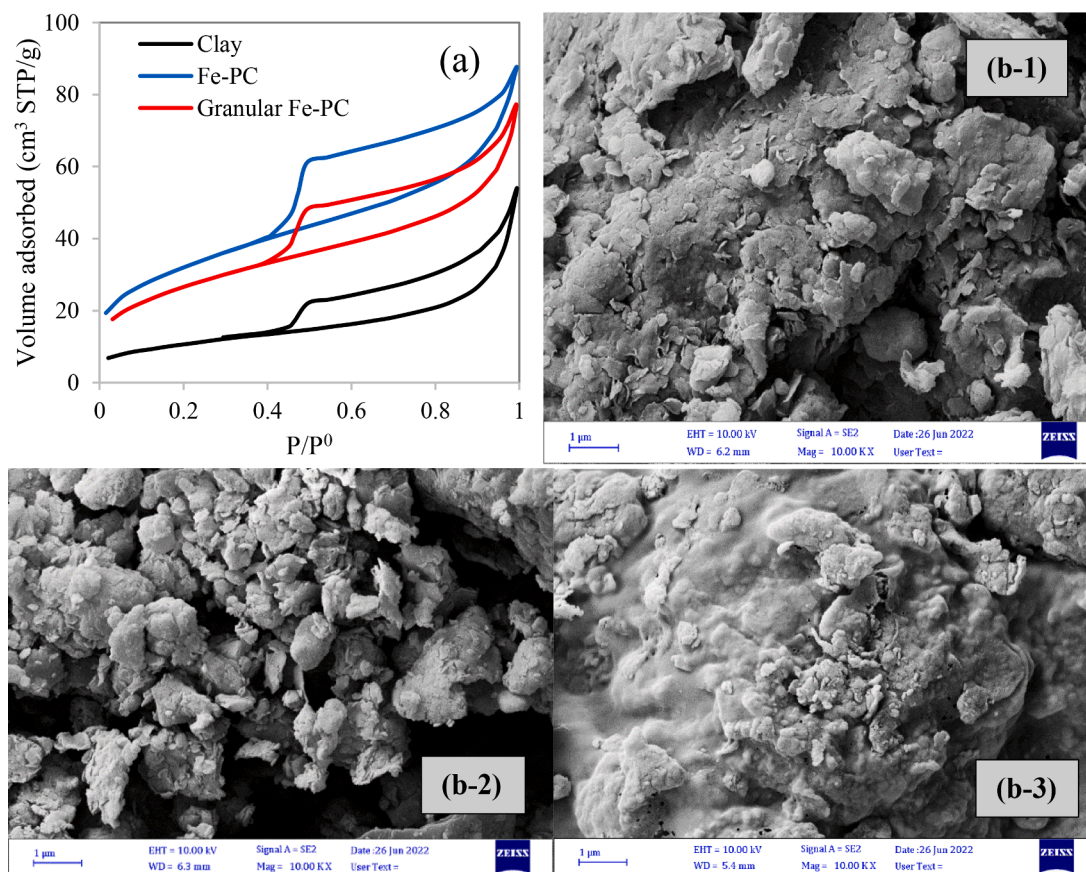


Fig. 4. (a) Nitrogen adsorption-desorption isotherms of the clay samples at 77 K and (b) FESEM micrographs showing (b-1) The raw clay (montmorillonite), (b-2) Fe-pillared clay, and (b-3) granular Fe-pillared clay.

Table 2

Porous properties of clay samples showing N_2 adsorption-desorption isotherm at 77 K.

Sample	Specific surface area (m^2/g)	Total pore volume (cm^3/g)	BJH mesopore volume (cm^3/g)	BJH mesopore width (Å)	Mesoporous percentage (%)
Clay (Mt)	38.1	0.083	0.082	38.6	99
Fe-PC	114.5	0.136	0.121	38.9	89
Granular Fe-PC	96.3	0.119	0.105	36.6	88

Zviagina et al. assigned the band at about $680\text{--}685\text{ cm}^{-1}$ to the out-of-plane Fe-O vibration [45]. It can be seen that all types of clays (Fe-treated and untreated) have the same shape, indicating that Fe-O cannot be detected by FTIR. However, a comparison of the FTIR spectra of the three sorbents shows no significant deviation in this area. Furthermore, the possibility of Fe-OH stretching vibrations cannot be accurately confirmed, as there are no significant differences in the intensity of the alcoholic bond peaks between pillared and raw clay.

To compare the acidity of the adsorbents, the pH_{pzc} (point of zero charge) of both Fe-PC and granulated Fe-PC samples was determined using the pH drift method and yielded values of 5.9 and 3.8, respectively. It is noteworthy that the addition of CMC during the granulation process introduced carboxyl groups ($-\text{COOH}$) into the structure of the pillared clays. Although CMC is a relatively neutral compound, the addition of acidic groups resulted in a decrease in pH_{pzc} for the granulated Fe-PC samples, ultimately leading to a decrease in this value compared to Fe-PC. These observations highlight the effect of CMC on the pH_{pzc} of the clay samples and illustrate the potential influence of

acidic groups on the adsorption behavior of these materials.

In contrast to FTIR, diffuse reflectance spectroscopy (DRS) analysis is effective in confirming the incorporation of Fe groups (iron), typically with an oxidation state of +3, into the clay structure by pillarization. The absorption spectra of both the raw clay and the Fe-pillared clay (Fe-PC) were measured in the wavelength range of $200\text{--}800\text{ nm}$, as shown in Fig. 6. The DRS spectra of the two clays showed significant differences. In particular, the Fe(III) species in the Fe-PC structure exhibited a strong absorption band in the visible region of $300\text{--}500\text{ nm}$, indicating the presence of Fe ions. These observations provide empirical evidence for the successful incorporation of Fe groups into the clay structure by pillarization.

3.2. Adsorption-desorption studies

3.2.1. Effect of adsorbent dosage

The aim of the first series of experiments was to compare the performance of powdered Fe-PC and granulated Fe-PC in the adsorption of Tc and Tz over a period of 0 to about 30 h. Fig. 7(a) and (b) show the kinetic behavior of the two forms of Fe-PC in the adsorption of Tc and Tz, respectively. It is clear that granulation has a significant effect on Tc adsorption kinetics, while the effect on Tz adsorption kinetics is relatively small. The slower kinetics observed for granulated PC can be attributed to the larger particle size, thicker boundary layer and higher mass transfer resistance compared to powdered Fe-PC. The equilibrium time for Tc adsorption is about 6 h for the powdered form, but increases to 30 h for the granulated form. However, once equilibrium is reached, there is no significant difference between the two forms of Fe-PC in terms of final removal percentage. In contrast, the kinetics for Tz is faster for powdered Fe-PC; the equilibrium time for both forms of Fe-PC is about 6 h. This discrepancy in kinetics can be attributed to the larger

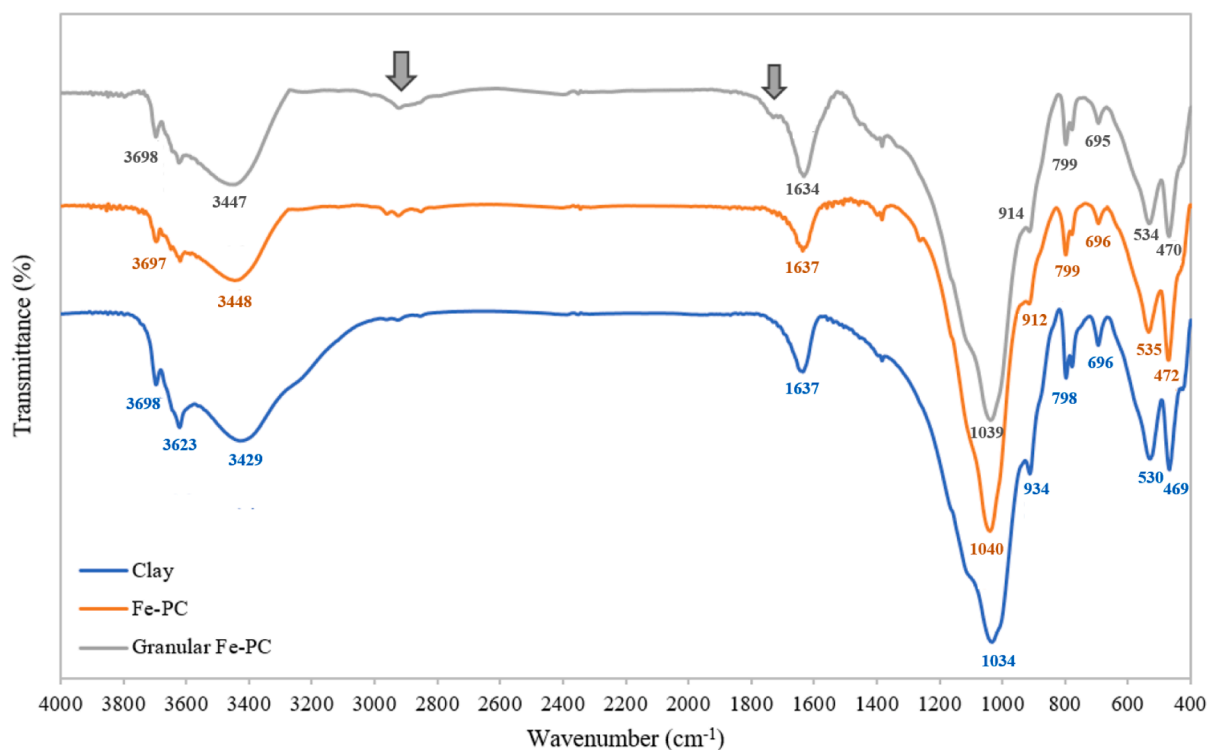


Fig. 5. FTIR spectra of montmorillonite clay, iron pillared clay in the powdered and granular forms.

Table 3

Identification of major bond peaks in FTIR spectra of clay samples.

Wavenumber (cm ⁻¹) (Peak intensity)	Bonds	Samples		
		Clay	Fe-PC	Granular Fe-PC
3623–3698 (medium, sharp), 3429–3448 (strong, broad)	O-H stretching, Alcohol	✓	✓	✓
2840–3000 (medium)	C–H stretching	×	×	✓
1700 (weak)	C = O stretching	×	×	✓
1634–1637 (medium)	O-H bending	✓	✓	✓
912–934 (weak)	Al–OH bending	✓	✓	✓
1034–1040 (strong); 798–799 (medium)	Si–O–Si, symmetric stretching	✓	✓	✓
695–696 (weak)	Al–O bending	✓	✓	✓
530–535 (medium)	Si–O stretching & Si–O–Si symmetric stretching	✓	✓	✓
469–470 (medium)	Si–O–Si out of plane	✓	✓	✓

molecular size and bulkier structure of Tc compared to Tz, which makes the adsorption of Tc at the active sites of granulated PC more difficult due to the higher mass transfer resistance.

The adsorption capacity of Fe-PC is primarily due to its porous texture and its inherent surface species and functional groups. The addition of CMC to granulated Fe-PC decreases its specific surface area and porosity, but adds some functionalities to the granulated Fe-PC surface. Therefore, the final removal percentages of both forms of Fe-PC were comparable, suggesting that CMC provides additional functionalities that compensate for the limitations of the porous properties by binding or reducing the accessibility of the active sites after granulation.

Despite the lower adsorption kinetics of granulated pillared clay, its superior mechanical strength, stability and ease of separation make it an attractive choice for many industrial applications. In addition, the ability to use the adsorbent in low pressure drop column systems highlights the practical advantages of granulated pillared clay. Considering

its industrial feasibility and reliable adsorption capacity, granular pillared clay was therefore selected for further experiments.

Fig. 8(a) and (b) show the influence of adsorbent dosage on the percentage of Tc and Tz removal and the respective adsorption capacities. The investigated dosage range for Tc and Tz was between 0.5–4 g/L and 0.5–3 g/L, respectively. It can be seen from the graph that the percentage removal, indicated by the blue bars, has an increasing trend for both contaminants as the dosage increases. At a certain point, however, the rate of increase decreases and the curves reach a plateau. Although it can be concluded that the values 3.5 and 2 are the lowest dosage values at which the percentage removal has reached a constant percentage, the values 3 and 1.5 were chosen as the optimal values in this study. The reason for this is that, in addition to the percentage of removal, economic aspects are also taken into account and the difference between the percentage of removal at these two dosage values is negligible. Choosing a lower dosage therefore helps to make the process more economically efficient.

The results show that an increase in the adsorbent dosage is accompanied by an increase in the removal percentage but a decrease in the adsorption capacity. The optimum adsorbent dosage for Tc and Tz was found to be 3 and 1.5 g/L, respectively. These results confirm the higher affinity of granulated Fe-PC to Tz compared to Tc under identical operating conditions.

3.2.2. Effect of pH

Fig. 9 illustrates the influence of pH on the percentage removal of Tc and Tz. The observed curve can be compared with the species distribution of Tc and Tz determined using the Henderson-Hasselbalch equation based on the pK_a values of Tz (7.5) and Tc (9.4, 7.3 and 3.3). This comparison allows the identification of the underlying mechanisms involved in the adsorption of each component [46], which is more explained in Section 3.2.5.

According to the results of the pH_{pzc} experiment, the granular adsorbent had a pH_{pzc} of 3.8, indicating that the surface of the adsorbent is negatively charged during the majority of the pH range (> 3.8), while at lower pH values the surface functional groups are protonated and

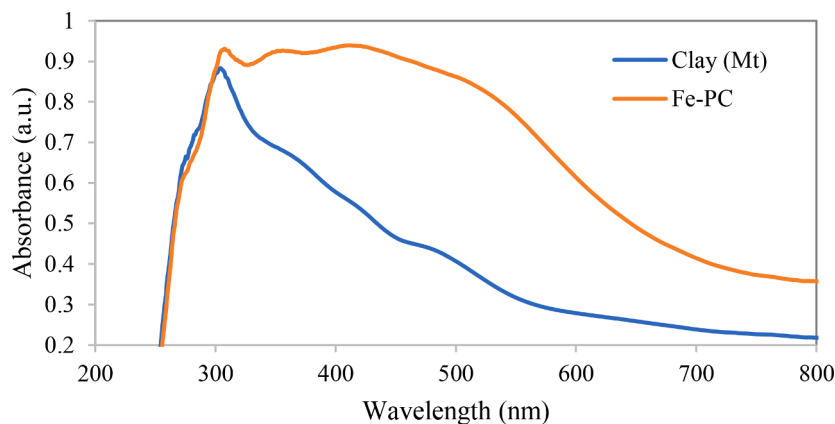


Fig. 6. Diffuse-reflectance UV-Vis spectra of the raw and Fe pillared clays.

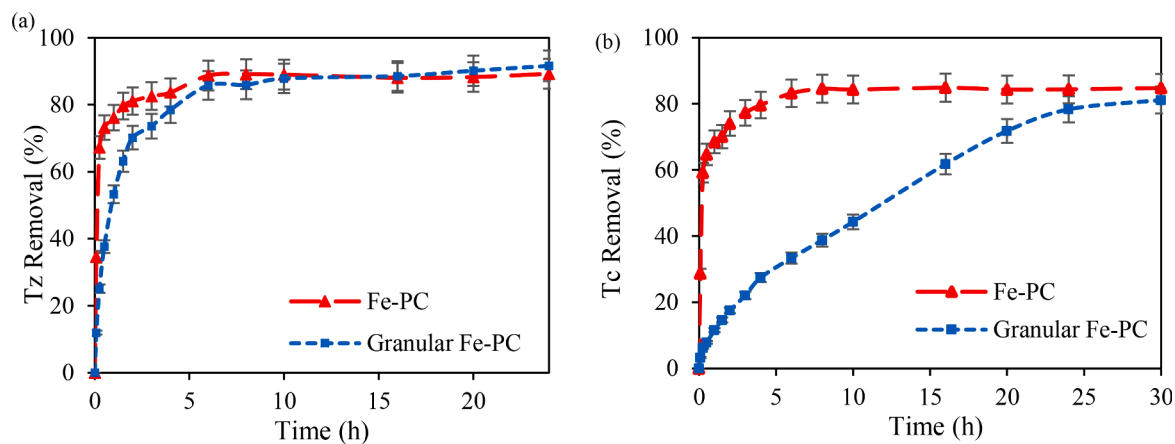


Fig. 7. A comparison of Tz and Tc removal rates by Fe-PC and granulated Fe-PC (Initial concentration of pollutant: 30 mg/L, adsorbent dosage: 3 g/L (for Tc) and 1.5 g/L (for Tz), pH: 7, and T: 30 °C).

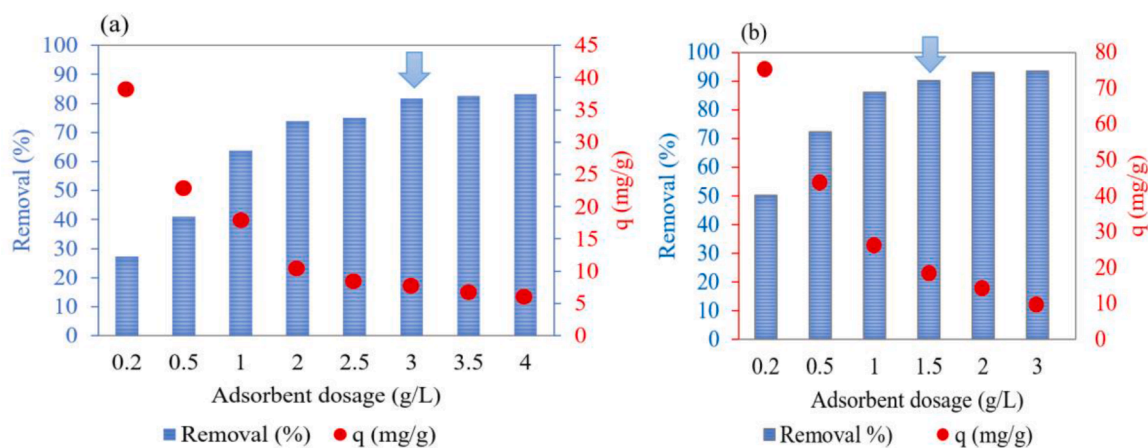


Fig. 8. Effect of granulated Fe-PC dosage on the adsorption of (a) tetracycline and (b) tizanidine (Initial concentration: 30 mg/L, pH: 7, contact time: 24 h, and T: 30 °C).

acquire a positive charge. The observed poor performance of the adsorbent in adsorbing Tc and Tz at very acidic pH values is attributed to the strong repulsion between the positively charged species of Tc and Tz and the positively charged surface of the adsorbent. Similarly, at very high pH values, the negatively charged surface of the adsorbent and the Tc species lead to weak adsorption due to the repulsive forces. However, the neutral form of Tz leads to weaker repulsion at high pH values

because it is predominantly present in a neutral molecular form. In addition, the negatively charged surface of the Tc species in a broader pH range leads to a less favorable adsorption affinity compared to the Tz species. This clear pH dependence confirms the crucial role of electrostatic adsorption, where both attractive and repulsive forces play a role in the adsorption mechanism of Tc and Tz compounds.

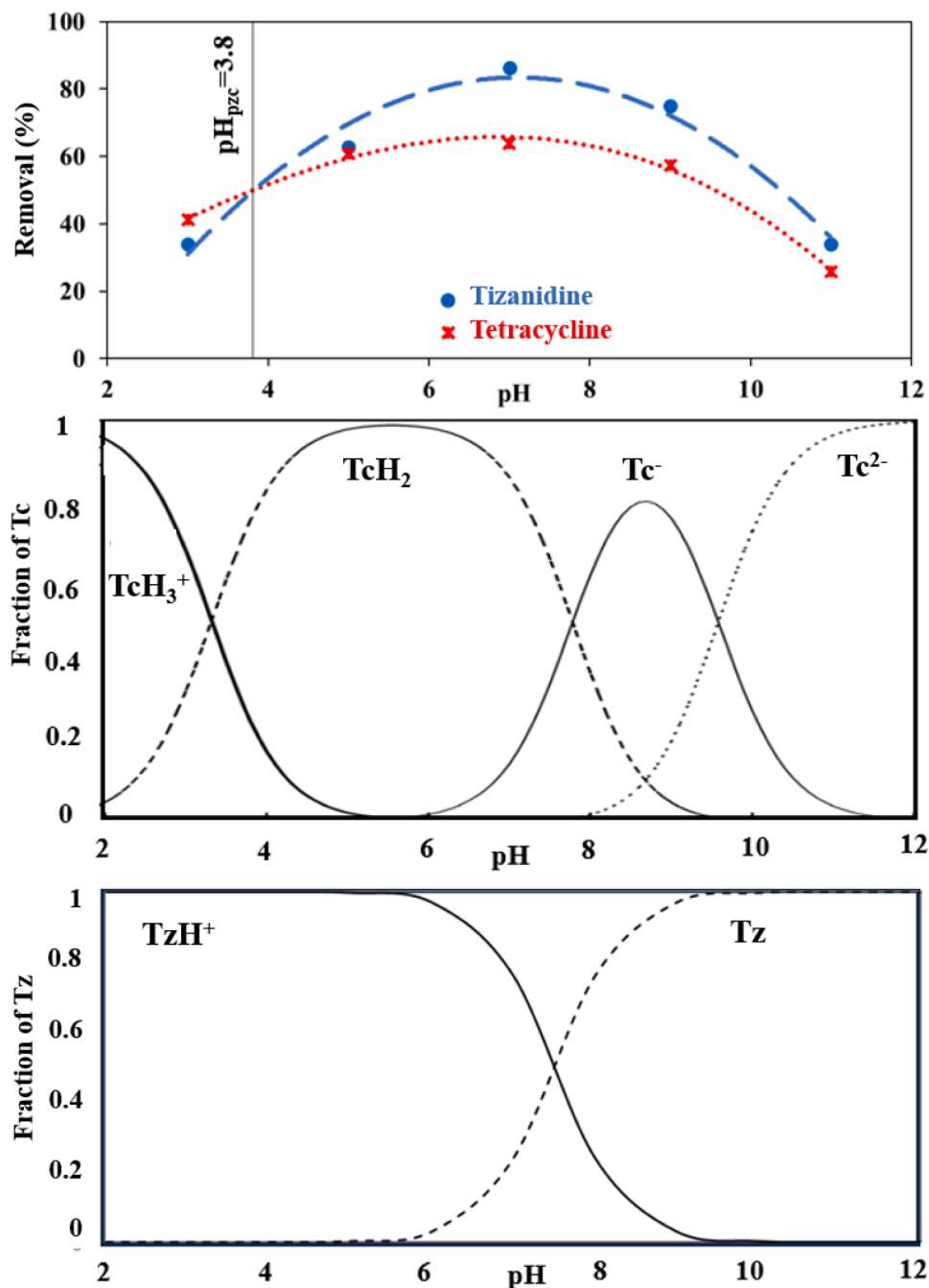


Fig. 9. The impact of pH on the percentage removal of Tz and Tc (Initial concentration: 30 mg/L, adsorbent dosage: 1 g/L, contact time: 24 h, and T: 30 °C), alongside their respective species distribution determined using the Henderson-Hasselbalch equation based on the pK_a s.

3.2.3. Adsorption kinetics

In this study, the kinetics of Tc and Tz adsorption by Fe-PC in powder and granular form were investigated using common chemical reaction-based kinetic models (pseudo-first order (PFO) [47] and pseudo-second order (PSO) [48]) and diffusion-based models (Weber & Morison model [49] and film diffusion model [50]). Part of the experimental data that was far from equilibrium was used for kinetic modeling to avoid the inclusion of the equilibrium data (Fig. 10). In both the PFO and PSO models, adsorption is treated as a chemical reaction without considering the diffusion of contaminants. The statistical parameters, including SSE (sum of squares error), R^2 (coefficient of determination) and RMSE (root mean square error), were calculated and presented in Table 4 to evaluate the fit of these models to the experimental data.

Our results showed that the PSO model with relatively higher R^2

values and lower RMSE and SSE values could better predict the adsorption of the two sorbates by the sorbents than the PFO model. In addition, $q_{e,exp}$ was found to be in better agreement with the $q_{e,model}$ predicted by the PSO model, emphasizing its superiority over the PFO model.

Additionally, the kinetic constants of the PSO model, namely the initial sorption rate (h) and the rate constant (k_2), were compared to quantify the difference between the adsorption rates of powdered and granular Fe-PC. The results showed that the sorption rate of powdered Fe-PC was about 87 times faster for Tc and 7 times faster for Tz compared to the granular sample.

In addition, the sorption rates of Tz and Tc by each type of sorbent were compared. The results showed that Tz was adsorbed faster than Tc with each type of sorbent. In particular, the sorption rate of Tz with

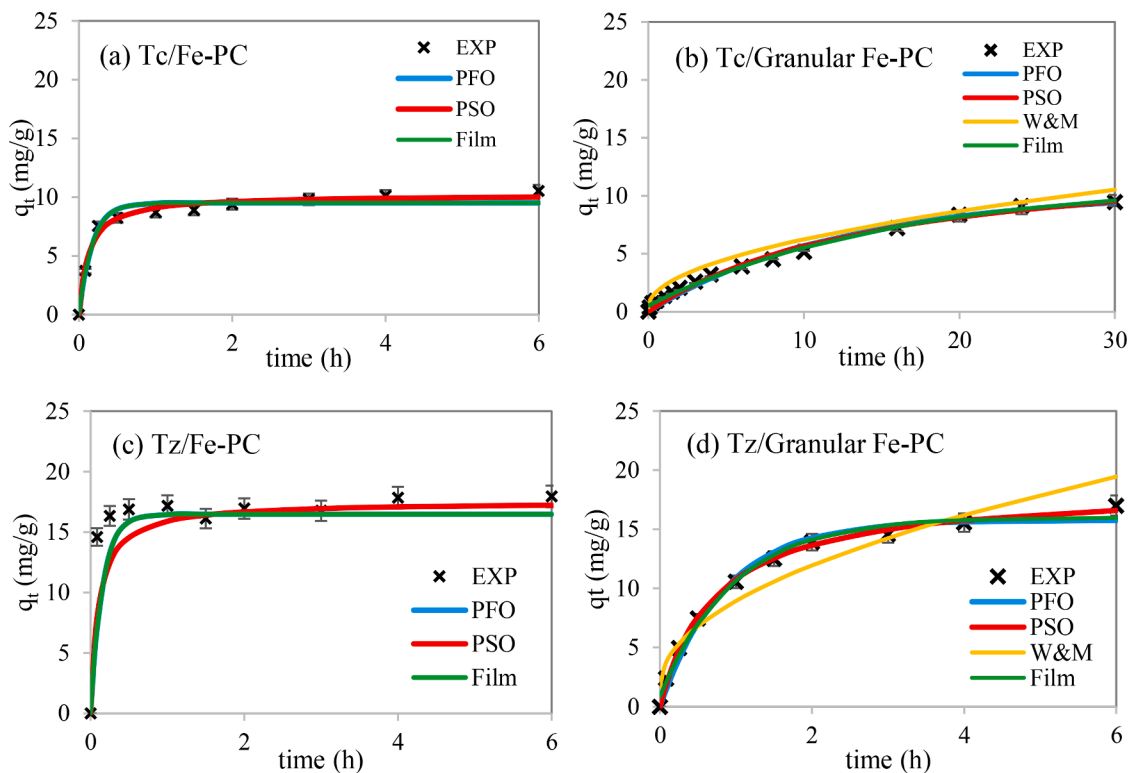


Fig. 10. Experimental kinetic curves and chemical reaction-based kinetic models (PFO and PSO) and diffusion models (W&M and Film diffusion) fitted to the experimental data.

Table 4

Comparison of kinetic and statistical parameters for Tc and Tz adsorption on the powdered and granular Fe-PC surfaces.

Tz/Granular Fe-PC	Tz/ Fe-PC	Tc/Granular Fe-PC	Tc/ Fe-PC	Equation	Kinetic model
18.2	18.0	>10	10.8	Experimental equilibrium capacity ($q_{e,exp}$)	18.2
Pseudo-first order	$q_t = q_e(1 - \exp(-k_1t))$	$k_1=5.73$ 1/h; $q_e=9.508$ mg/g; SSE= 3.082; $R^2=0.9689$; RMSE=0.6207	$k_1= 0.081$ 1/h; $q_e=10.3$ mg/g; SSE= 2.367; $R^2=0.9846$; RMSE=0.4112	$k_1=6.544$ 1/h; $q_e=16.47$ mg/g; SSE= 4.881; $R^2=0.983$; RMSE=0.7811	$k_1=1.175$ 1/h; $q_e=15.77$ mg/g; SSE= 4.569; $R^2=0.9854$; RMSE=0.7557
Pseudo-second order	$q_t = \frac{k_2q_e^2t}{1 + k_2q_e t}$	$k_2= 0.7896$ g/mg.h; $q_e=10.214$ mg/g; $h = 82.37$ mg/g.h; SSE= 1.431; $R^2=0.9855$; RMSE=0.423	$k_2= 0.0046$ g/mg.h; $q_e=14.3$ mg/g; $h = 0.94$ mg/g.h; SSE= 1.862; $R^2=0.9879$; RMSE=0.3647	$k_2= 0.5564$ g/mg.h; $q_e=17.52$ mg/g; $h = 170.79$ mg/g.h; SSE= 3.149; $R^2=0.989$; RMSE=0.6274	$k_2= 0.0742$ g/mg.h; $q_e=18.59$ mg/g; $h = 25.62$ mg/g.h; SSE= 0.7415; $R^2=0.9973$; RMSE=0.3044
Weber & Morris Model	$q_t = K_p t^{0.5} + C$	$K_p=3.524$ mg/g.h ^{0.5} ; $C = 3.704$ mg/g; SSE=30.35; $R^2=0.6934$; RMSE=1.948	$K_p=1.85$ mg/g.h ^{0.5} ; $C=-0.3947$ mg/g; SSE=1.2; $R^2=0.9922$; RMSE=0.2928	$K_p=5.735$ mg/g.h ^{0.5} ; $C = 6.997$ mg/g; SSE=104.8; $R^2=0.6343$; RMSE=3.62	$K_p=7.251$ mg/g.h ^{0.5} ; $C = 1.691$ mg/g; SSE=22.15; $R^2=0.9292$; RMSE=1.664
Pseudo-first order	$q_t = q_e(1 - \exp(-(k_f t + A)))$	$q_e=9.512$ mg/g; $k_f=5.649$ 1/h; $A = 0.009606$; SSE= 3.074; $R^2=0.969$; RMSE=0.6626	$q_e=11.2$ mg/g; $k_f=0.0632$ 1/h; $A = 0.04836$; SSE= 0.9155; $R^2=0.9941$; RMSE=0.2654	$q_e=16.47$ mg/g; $k_f=6.502$ 1/h; $A = 0.004761$; SSE= 4.874; $R^2=0.983$; RMSE=0.8345	$q_e=16$ mg/g; $k_f=1.043$ 1/h; $A = 0.0548$; SSE= 3.241; $R^2=0.9867$; RMSE=0.6804

powdered Fe-PC was about two times higher than that of Tc, while the sorption rate of Tz with granulated Fe-PC was 27 times higher than that of Tc.

The results show that the effect of granulation on the adsorption rate of Tz was relatively small compared to Tc. This may be attributed to the bulkier molecular structure of Tc, which makes it more difficult to diffuse and adsorb into the pores of the granulated adsorbent. The lower adsorption rate for Tc can therefore be attributed to the hindered diffusion due to its molecular size and shape.

To gain further insight, a study of diffusion-based kinetic models was

conducted to determine the predominant diffusion mechanisms involved in the adsorption process. The Weber & Morris intraparticle model was analyzed and found to provide an acceptable fit only for the adsorption of Tc and Tz on the granular Fe-PC. The adequacy of this model in capturing intraparticle diffusion as a mechanism contributing to adsorption was demonstrated, although it should be noted that the non-zero intercept of this model indicates that intraparticle diffusion is not the only mechanism involved in the adsorption process [49]. For the powdered sorbent, due to the extremely fine particle sizes of Fe-PC and the accessibility of the active sites, the intraparticle mass transfer

resistance was found to be negligible. As a result, this model did not fit this particular scenario well.

The application of the film diffusion model showed good agreement for all adsorption systems and resulted in a higher film diffusion mass transfer coefficient for the powdered sample compared to the granular sorbent. These findings underscore the complex diffusion mechanisms at play during the adsorption process. For granular Fe-PC, intraparticle diffusion should be emphasized, while both granular and powder sorbent samples exhibit significant film diffusion. In particular, film diffusion is much faster in powdered Fe-PC than in its granular form.

3.2.4. Equilibrium and thermodynamic studies

The equilibrium adsorption experiments were carried out at different initial concentrations and three different temperatures (308 K, 318 K and 328 K). The experimental isotherm data obtained were fitted to two adsorption models: the Langmuir and Freundlich models, as shown in Fig. 11. Table 5 lists the isotherm parameters together with statistical indicators that quantify the agreement between the models and the experimental data. These models are widely used in different adsorption

systems and provide valuable quantitative insights for the comparison of different systems.

The Langmuir model, for example, is known for its key assumptions, including monolayer adsorption and homogeneous surface sites that are energetically equivalent and function independently. The maximum monolayer adsorption capacity (q_m) is a fundamental property of the Langmuir isotherm that provides an estimation of the accessible surface area for sorbates. In contrast, the Freundlich isotherm assumes that the surface sites on the adsorbent are heterogeneous, implying different energies for adsorption.

In the present study, the Langmuir isotherm outperformed the Freundlich model in the adsorption of Tc on granular Fe-PC, indicating a relatively homogeneous adsorption surface. For the adsorption of Tz on granular Fe-PC, the Freundlich model performed better than the Langmuir model, especially at high equilibrium concentrations where the predictions of the Langmuir model were remarkably weak in terms of adsorption capacities. When comparing the statistical parameters, it becomes clear that the Freundlich model has higher R^2 values and a lower SSE and RMSE in the case of Tz adsorption, and vice versa about

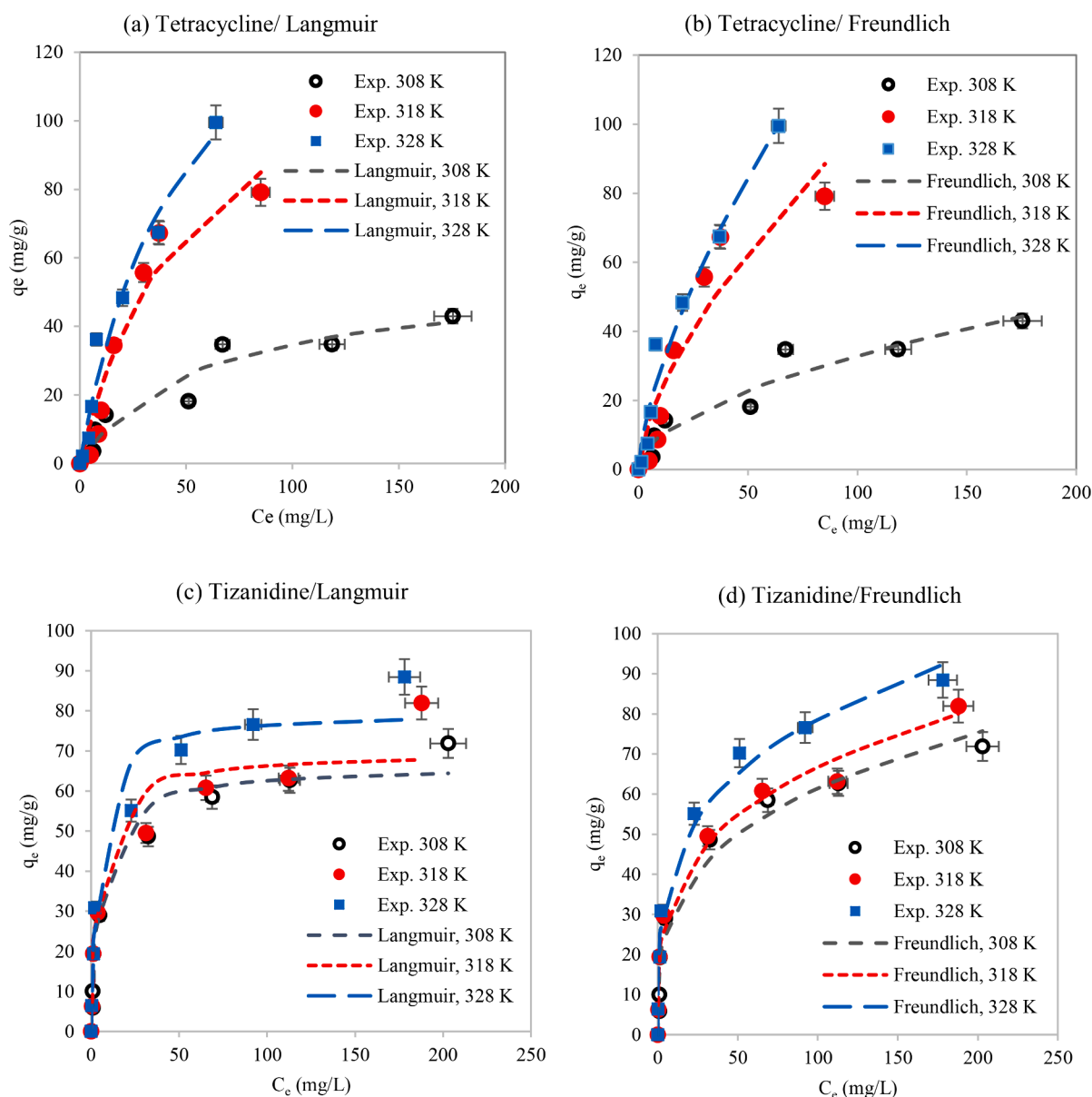


Fig. 11. Equilibrium isotherm data for tetracycline (Tc) and tizanidine (Tz) adsorption onto granular Fe-PC at three different temperatures (308 K, 318 K, and 328 K) fitted using two isotherm models (Langmuir, and Freundlich).

Table 5
The isotherm models parameters fitted to the equilibrium adsorption data at different temperatures.

Isotherm model	Equation	Temperature Adsorbent	308 K	318 K	328 K
Langmuir	$q_e = \frac{q_{m,L}K_L C_e}{1 + K_L C_e}$	Tc/Granular Fe-PC	$q_{m,L} = 54.89$ mg/g; $K_L = 0.0173$ L/mg; SSE=134.6; $R^2=0.934$; RMSE=4.385	$q_{m,L} = 137.62$ mg/g; $K_L = 0.0189$ L/mg; SSE=421.6; $R^2=0.9374$; RMSE=8.383	$q_{m,L} = 169.38$ mg/g; $K_L = 0.0206$ L/mg; SSE=250; $R^2=0.9716$; RMSE=6.454
Freundlich	$q_e = K_F C_e^{1/n}$		$K_F = 2.845$ (mg/g)/(L/mg) ^(1/n) ; $n = 1.882$; SSE=140; $R^2=0.9314$; RMSE=4.772	$K_F = 5.105$ (mg/g)/(L/mg) ^(1/n) ; $n = 1.558$; SSE= 763.9; $R^2= 0.8866$; RMSE= 11.28	$K_F = 6.167$ (mg/g)/(L/mg) ^(1/n) ; $n = 1.493$; SSE= 258; $R^2= 0.9707$; RMSE= 6.557
Langmuir	$q_e = \frac{q_{m,L}K_L C_e}{1 + K_L C_e}$	Tz/Granular Fe-PC	$q_{m,L} = 66.40$ mg/g; $K_L = 0.1604$ L/mg; SSE=175.3; $R^2=0.9699$; RMSE=5.004	$q_{m,L} = 69.71$ mg/g; $K_L = 0.1908$ L/mg; SSE=376.8; $R^2=0.938$; RMSE=7.925	$q_{m,L} = 79.67$ mg/g; $K_L = 0.2337$ L/mg; SSE=310.9; $R^2=0.961$; RMSE=7.198
Freundlich	$q_e = K_F C_e^{1/n}$		$K_F = 15.43$ (mg/g)/(L/mg) ^(1/n) ; $n = 3.34$; SSE=192.2; $R^2=0.967$; RMSE=5.241	$K_F = 17.49$ (mg/g)/(L/mg) ^(1/n) ; $n = 3.443$; SSE=117.6; $R^2=0.9806$; RMSE=4.428	$K_F = 22.01$ (mg/g)/(L/mg) ^(1/n) ; $n = 3.614$; SSE=141.2; $R^2=0.9793$; RMSE=4.852

Tc adsorption. This means that Tc adsorption occurs mainly in the form of a monolayer driven by chemical interactions between the adsorbate and the surface of the adsorbent. In contrast, when Tz is adsorbed, this molecule can be adsorbed in multiple layers, and the interaction between the adsorbate molecules plays an important role in the adsorption of Tz.

Accordingly, the results obtained from the Langmuir model may not accurately reflect the actual behavior of the adsorbent in the case of Tz adsorption. For instance, it can be observed that the maximum monolayer adsorption capacity at three different temperatures (308 K, 318 K, and 328 K) was approximately 55, 138, and 169 mg/g for Tc and 66, 70, and 80 mg/g for Tz. These results especially at higher temperatures are in contrast to the expected results considering the higher affinity of Tz for adsorption.

It can be observed that the maximum monolayer adsorption capacity (q_m) of granulated Fe-PC at low temperatures is greater for Tz than for Tc. At higher temperatures, however, Tc is adsorbed with a higher capacity than Tz. This behavior can also be observed by a qualitative comparison of the isotherm curves. The higher maximum adsorption capacity of the granular sorbent for Tz compared to Tc, similar to the higher kinetic rate of adsorption at lower temperatures, can be attributed to the smaller size of the Tz molecule and the presence of more active functionalities, resulting in a higher affinity of this component for adsorption.

It has also been observed that an increase in temperature increases the adsorption capacity for both Tz and Tc. This indicates that adsorption is based on an endothermic mechanism. However, the positive effect of temperature on the adsorption capacity of Tc is significantly greater than that of Tz, which means that the adsorption of Tz is less sensitive to temperature. Consequently, the adsorption capacity for Tc at sufficiently high temperatures is much higher than that for Tz under the same operating conditions. This indicates that the adsorption of Tc becomes more competitive and superior to that of Tz when the temperature is significantly increased. In addition, increasing the temperature resulted in a relatively higher K_L value, with higher K_L values indicating stronger adsorption, while lower values indicate weaker adsorption.

The thermodynamic parameters for the adsorption processes, including the changes in Gibbs free energy (ΔG , kJ/mol), the changes in enthalpy during adsorption (ΔH , kJ/mol), and the changes in entropy (ΔS , kJ/mol·K), were determined using the following equation:

$$\Delta G = \Delta H - T\Delta S = -RT \ln K \tag{3}$$

In our analysis, the standard equilibrium constant calculated from

the experimental equilibrium constant is used as K.

$$K = K_d \times \frac{C^0}{q^0} = \frac{q_e}{C_e} \times \frac{C^0}{q^0} \tag{4}$$

K_d has the unit of L/kg, and according to the IUPAC regulations, C^0 is chosen as 1 mol/L and when the adsorbate is not a gas, the value of 1 mol/kg is suggested for q^0 [51]. Table 6 contains all the thermodynamic parameters for both adsorption systems.

Table 6 shows that the adsorption process of both species on granular Fe-PC exhibits a negative change in Gibbs free energy, indicating its spontaneity. The magnitudes of ΔG for both adsorption systems are similar. The observed endothermic properties, as previously noted in our isotherm curves, indicate that an external heat input is necessary to improve the efficiency of the adsorption process, with better performance at higher temperatures. The lower ΔH values for the Tz adsorption system confirm its lower sensitivity to temperature changes.

In addition, a positive entropy change was observed in both adsorption systems, indicating an increase in randomness at the solid-solution interface during the adsorption process. This phenomenon can be attributed to structural changes in the adsorbed species and could also be related to the translational entropy of the desorbed molecules [52].

3.2.5. Adsorption mechanism

To further investigate the adsorption mechanisms of tetracycline, FTIR analysis of granular Fe-PC before and after tetracycline adsorption was performed and these spectra were compared with pure tetracycline (Fig. 12(a)). The spectra of granular Fe-PC before and after tetracycline adsorption showed no additional peaks, but an increase in peak intensity was observed after adsorption. A notable difference between granular Fe-PC before and after tetracycline adsorption was the increase in bond intensity in the range of 3450–3700 cm^{-1} , which could be due to the detection of more -OH stretching bonds added by the tetracycline structure [53]. In addition, we found an increase in the intensity of small absorption peaks at around 2870 and 2930 cm^{-1} in Fe-PC saturated with

Table 6
The thermodynamic parameters of Tc and Tz adsorption onto granular Fe-PC.

Adsorbate/ Adsorbent	ΔH (kJ/ mol)	ΔS (kJ/mol. K)	ΔG (kJ/mol)		
			308 K	318 K	328 K
Tc/Granular Fe-PC	77.91	0.2997	-14.40	-17.40	-20.40
Tz/Granular Fe-PC	14.24	0.0951	-15.06	-16.01	-16.96

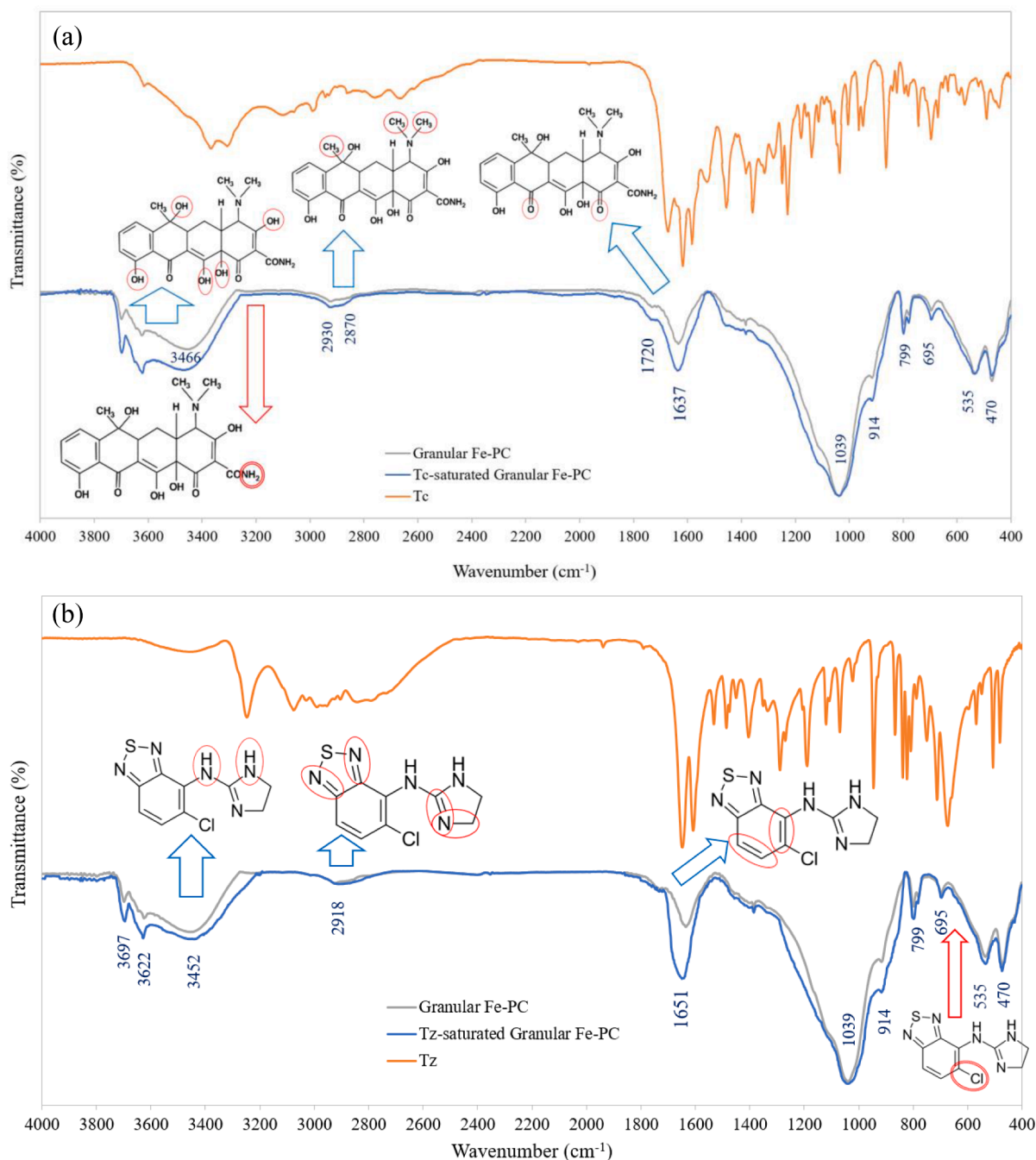


Fig. 12. FTIR spectra of (a) pure Tc adsorbate, granular Fe-PC, and Tc-saturated adsorbent, and (b) pure Tz adsorbate, granular Fe-PC, and Tz-saturated adsorbent. The two-line circle highlights the functional groups entirely involved in adsorption, while the one-line circle denotes those partially engaged in adsorption.

tetracycline, which are attributed to C—H stretching [54]. These observations indicate that the surface of the granular Fe-PC is coated with the free CH₃ groups of the adsorbed tetracycline. Although the presence of the amino group (-NH₂) of tetracycline typically leads to a peak in the tetracycline spectra in the range of 3200–3500 cm⁻¹ [55], this peak was not present in the case of the saturated adsorbent, suggesting that all the NH₂ groups of tetracycline were involved in its adsorption. This wavenumber range is related to the vibrational bands of the N—H bond and the -NH₂ group, as observed by Trivedi et al. [53] for tetracycline and chloramphenicol and by Guo et al. [56] for NH₂-MIL-88. In addition, the peak of the carbonyl group (C = O) appeared in the spectrum of tetracycline at 1650–1750 cm⁻¹ [53], and a slight increase in peak intensity was observed in the spectra of saturated Fe-PC in this region, indicating that only part of the carbonyl, carboxyl, and hydroxyl groups

were involved in the adsorption and reaction processes.

There are two different amino groups in the molecular structure of tizanidine, including -NH₂ with a characteristic peak in the range of 3200–3500 cm⁻¹, corresponding to N—H stretching, and a secondary amino group (N—CH₃) with a characteristic peak around 2800–3000 cm⁻¹, corresponding to C—H stretching in CH₃ groups. These functional groups contribute significantly to the spectral peaks observed in tizanidine. The partial involvement of amino groups in the adsorption of Tz could explain the slight shift of the granulated Fe-PC peaks located in the high wavenumber region (~3452 cm⁻¹) as well as the slight increase in the intensity of the peak at 2918 cm⁻¹. The presence of C = C bonds in the tizanidine molecule also leads to a relatively robust peak in the spectrum in the 1600–1650 cm⁻¹ region, and the adsorption of Tz on the surface of granulated Fe-PC leads to an increase in the intensity of the

peak at 1651 cm^{-1} , which specifically corresponds to the free $\text{C}=\text{C}$ bonds in the heterocyclic rings of the molecule. In addition, subtle differences are observed in the spectra of the granulated fresh sorbent compared to the Tz-sorbed sorbent in the $1200\text{--}1300\text{ cm}^{-1}$ range, possibly due to the presence of $\text{C}-\text{N}$ bonds. From the FTIR analysis, it can be concluded that the amino groups are the primary functional groups involved in the adsorption of tizanidine on the surface of the sorbent. Alternatively, the presence of the $\text{C}-\text{Cl}$ bond in the structure of Tz leads to intense peaks at 660 cm^{-1} that are not seen in the spectra of granular Fe-PC. The absence of this peak in the case of the saturated adsorbent indicates that the bond is fully involved in the adsorption process, suggesting an interaction between the substrate and the adsorbate.

3.2.6. Desorption studies and cyclic performance

Another approach to elucidate the underlying mechanisms is to study the desorption of adsorbed species. Desorption was thoroughly investigated by evaluating the cyclic performance of the adsorbent through five consecutive adsorption-desorption experiments (Fig. 13). In the first adsorption step, the granular Fe-PC showed the ability to adsorb Tc and Tz to the extent of 75 % and 93 %, respectively. HCl (0.1 M), NaCl (0.1 M) and ethanol solutions were used as eluents.

The effectiveness of acidic and alkaline solutions in desorbing species from the surface of the adsorbent is usually based on the influence of pH on adsorption, especially for metal cations [57]. Since metal cations tend to precipitate at higher pH values, acidic eluents are more commonly used than alkaline ones. However, our study considers the effects of both types of pH modifiers. Ethanol has been used as a successful eluent for the desorption of organics such as Remazol Red [58] and methyl orange [59] from chitosan-treated cotton composites, and at the same time serves both as a desorbing agent and as a regenerator for the adsorbent.

The eluents showed different behavior with respect to the desorption of Tc and Tz, which had a significant impact on the adsorption capacity

of the recovered sorbent. An HCl solution (0.1 M) proved to be the most effective eluent for cyclic Tc adsorption. It not only facilitated desorption, but also increased the adsorption percentage of the regenerated adsorbent. Under the acidic conditions provided by this desorbing agent, competition occurred between H^+ and the positively charged species of Tz and Tc, which promoted the desorption of these compounds. However, in the adsorption of Tz, HCl treatment was not an effective recovery agent, suggesting that different mechanisms underlie the adsorption of Tc and Tz. Tc is favored by the presence of acidic functional groups, whereas the adsorption of Tz relies more on N-functionalities, which are not affected by HCl treatment.

Ethanol, on the other hand, was successful in desorbing Tc, but only retained the adsorption capacity of granulated Fe-PC in subsequent adsorption cycles. Conversely, NaCl was not promising in terms of adsorbent regeneration and Tc desorption. However, it proved to be the most effective agent for the regeneration of the granular adsorbent after Tz adsorption. The effectiveness of NaCl as a desorbing agent for the cationic Tz suggests that cation exchange is indeed one of the most important mechanisms in the adsorption of this species [30].

Based on the experiments and characterizations performed, we can draw conclusions regarding the primary mechanisms controlling the adsorption of Tc and Tz on granular Fe-PC. Electrostatic interactions play a crucial role in the adsorption of both Tc and Tz, as shown by the pH-dependent experiments and the repulsion of positively charged species from the adsorbent surface under strongly acidic conditions. In the case of Tz, the involvement of cation exchange as a concurrent mechanism is evident. This is supported by the remarkable performance of NaCl as a desorbing agent for Tz. This dual action, involving electrostatic interactions and cation exchange, highlights the complexity of the adsorption process for Tz.

Complexation is another important mechanism that plays a role in the adsorption of Tc and Tz. This is evidenced by the interaction of the NH_2 group of Tc and the amine and chloride groups of Tz with the

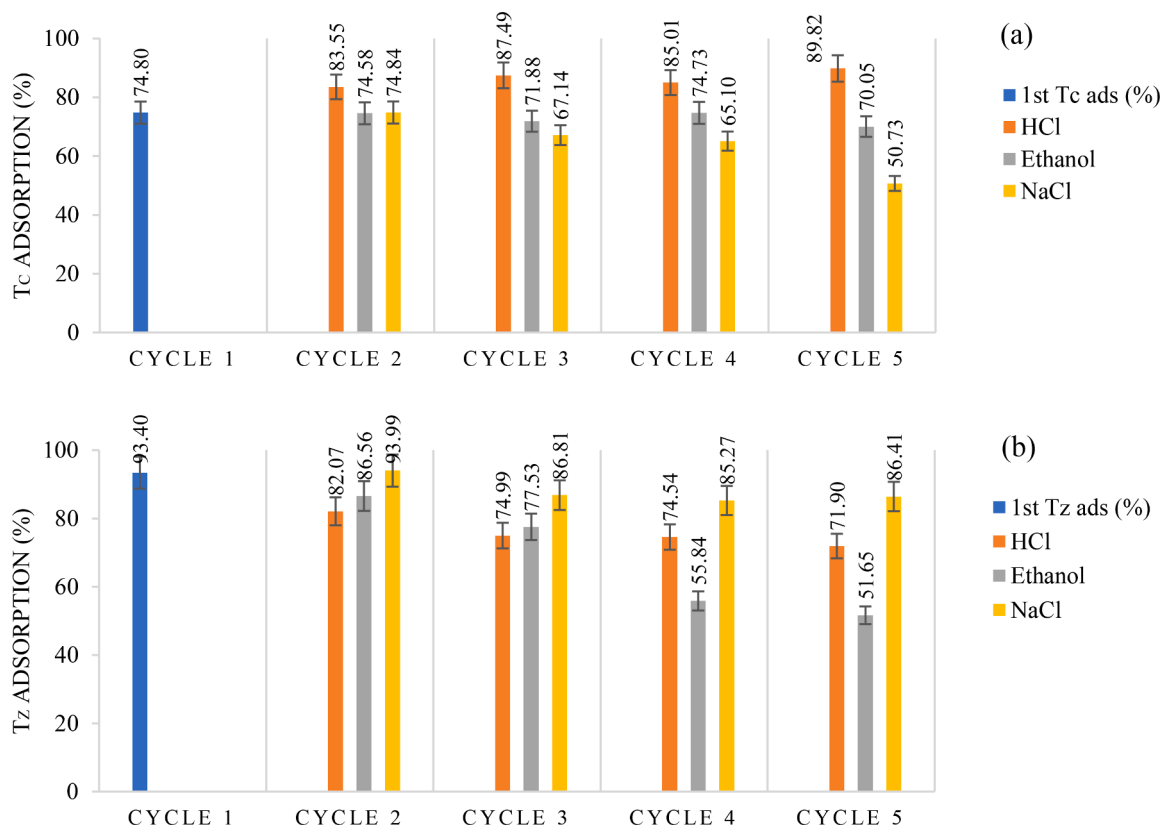


Fig. 13. The cyclic performance of granular Fe-PC in successive adsorption-desorption cycles by various eluting agents, (a) for Tc and (b) for Tz.

adsorbent by complexation, which is confirmed by FTIR studies. In the case of Tc, the oxygen-containing functional groups, such as carbonyl, carboxyl and hydroxyl groups, also play a partial role in the adsorption process. This is confirmed by cyclic adsorption-desorption experiments, where HCl proved to be the most effective eluent for the desorption of Tc and the regeneration of granular Fe-PC for subsequent Tc adsorption. Various complexation mechanisms may be involved, including π - π interactions between π -electron acceptors and donors, n - π interactions between electron pairs and electron-deficient aromatic rings of the adsorbate, and hydrogen bonding between the protons of electronegative atoms and the lone pair electrons of other electronegative atoms.

3.2.7. Multicomponent adsorption

Finally, competitive adsorption experiments were performed to evaluate the relative adsorption capacities of Tz and Tc in a binary aqueous system under realistic conditions. The adsorption results of Tz and Tc in single and binary systems were compared in Table 7, which includes two additional parameters for quantitative analysis. These parameters were the loss of adsorption in the binary system compared to the individual system and the superiority of the adsorption capacity of Tz over that of Tc. These were calculated using Eqs. (5) and (6):

$$\text{Loss of adsorption in binary system} = 100 \times \left(\frac{q_{\text{binary}} - q_{\text{single}}}{q_{\text{single}}} \right) \quad (5)$$

$$\text{Superiority of Tz to Tc adsorption} = 100 \times \left(\frac{q_{\text{Tz}} - q_{\text{Tc}}}{q_{\text{Tc}}} \right) \quad (6)$$

The results showed that the adsorption capacity of granular Fe-PC decreased for both adsorbates in the binary system compared to the corresponding values in the single-component system. The loss of adsorption for Tz ranged from 0.7 % to 15 %, while for Tc it ranged from 5 % to 32 %. However, increasing the dosage of adsorbent in the solution reduced the loss of adsorption. At the highest dosage of 3 g/L, similar adsorption capacities were observed for Tc in both single and binary systems. This indicates that the limited availability of adsorption sites resulted in greater competition between Tc and Tz at lower dosages of adsorbents.

The superiority of adsorption of Tz over Tc by granular Fe-PC was also investigated. The results showed that this superiority increased in the competing system under all conditions. However, increasing the adsorbent dosage led to a decrease in this superiority. Since sufficient adsorption sites are available, all adsorbates can be adsorbed regardless of their affinity. In summary, the performance of the granular Fe-PC adsorbent is maintained even under competitive conditions.

4. Conclusions

In the search for novel, cost-effective and practical adsorbents for the removal of pharmaceutical pollutants (tetracycline (Tc) and tizanidine (Tz)) from aqueous solutions, a type of Fe-pillared clay was introduced. The use of carboxymethylcellulose (CMC) as a binder for the granulation

of powdered Fe-pillared montmorillonite was studied. Analytical techniques, including XRF and DRS, confirmed the successful incorporation of Fe into the montmorillonite structure. FTIR and LOI tests confirmed the addition of CMC into the granular Fe-pillared clay. An increase was observed in porosity during pillaring (S_{BET} increased threefold), which was partially masked by CMC granulation. The equilibrium time for Tc adsorption increased as a result of granulation, while the kinetics of Tz were less affected. Importantly, the final percentage of removal showed no significant difference. Langmuir isotherm model was more suitable for Tc adsorption on granular Fe-pillared clay, while the Freundlich model was more suitable for Tz adsorption. Moreover, the pseudo-second order model could predict the adsorption kinetics better than the pseudo-first order model. Tz exhibited faster adsorption kinetics than Tc, primarily due to the bulkier molecular structure of Tc. In addition to film diffusion, intraparticle diffusion played an important role in adsorption by the granular adsorbent, whereas only film diffusion appeared to be involved for the powdered form. Investigation of pH effects revealed that electrostatic interactions played a central role in the adsorption of Tc and Tz. Complexation was also observed, with NH_2 groups and part of the oxygen-containing groups in Tc and amino groups in Tz being involved in the adsorption process. Effective desorbing agents were identified, with HCl proving effective for cyclic Tc desorption and NaCl for Tz desorption, indicating the importance of cation exchange in the adsorption of Tz. The adsorption processes were spontaneous and endothermic, with positive ΔS indicate increased randomness at the solid-solution interface. Finally, our study of competitive adsorption showed that Tz has a higher adsorption capacity compared to Tc in both single and binary systems. The dosage of adsorbent played an important role in the competition between Tz and Tc, with higher dosages leading to a decrease in the superiority of Tz over Tc and vice versa. This study provides valuable insights into the complex adsorption behavior of Tc and Tz on modified clay-based adsorbents, which has not been investigated before.

CRedit authorship contribution statement

Hanieh Khoshima Bazkiaee: Writing – original draft, Investigation, Data curation. **Seyedmehdi Sharifian:** Writing – original draft, Supervision, Methodology, Conceptualization. **Neda Asasian-Kolur:** Writing – original draft, Supervision, Methodology, Conceptualization. **Hanieh Najafi:** Investigation, Formal analysis. **Azadeh Ebrahimiyan Pirbazari:** Supervision, Methodology, Conceptualization. **Michael Harasek:** Supervision, Project administration, Conceptualization.

Declaration of competing interest

The authors declare that they have no known competing financial interests or personal relationships that could have appeared to influence the work reported in this paper.

Table 7

Comparison of the adsorption capacities of granular Fe-PC towards Tc and Tz in single- and competitive adsorption systems (Initial concentration: 30 mg/L (in single-component system) and 30 g/L (for each species in the binary system), pH=7, contact time= 24 h and temperature=25 °C).

Dosage (g/L)	q_{Tz} (mg/g) in		q_{Tc} (mg/g) in		Superiority of Tz to Tc adsorption in		Loss of Tz adsorption in binary system	Loss of Tc adsorption in binary system
	single-component system	binary system	single-component system	binary system	single-component system	binary system		
0.2	75.07	63.78	38.15	31.56	96.78	102.09	-15.04	-17.27
0.5	43.35	41.73	22.82	15.77	89.97	164.55	-3.74	-30.87
1	25.79	25.12	17.82	12.04	44.70	108.62	-2.59	-32.43
1.5	18.01	17.81	10.115	8.59	78.05	107.46	-1.10	-15.12
2	13.93	13.71	8.732	8.29	59.56	65.30	-1.63	-5.05
3	9.34	9.268	7.61	7.70	22.74	20.29	-0.78	1.24

Data availability

Data will be made available on request.

Acknowledgement

The authors acknowledge TU Wien Bibliothek for financial support through its Open Access Funding Programme.

Supplementary materials

Supplementary material associated with this article can be found, in the online version, at doi:10.1016/j.apsadv.2024.100600.

References

- [1] K. Samal, S. Mahapatra, M.H. Ali, Pharmaceutical wastewater as Emerging Contaminants (EC): treatment technologies, impact on environment and human health, *Energy Nexus* 6 (2022) 100076.
- [2] H. Jiang, X. Li, Y. Dai, Phosphoric acid activation of cow dung biochar for adsorbing enrofloxacin in water: icing on the cake, *Environ. Pollut.* 341 (2024) 122887.
- [3] S. Ghanavati, A. Derian, Tizanidine, in: *statPearls* [Internet], StatPearls Publishing (2022).
- [4] M.P.C. Mora-Gamboa, S.M. Rincón-Gamboa, L.D. Ardila-Leal, R.A. Poutou-Piñales, A.M. Pedroza-Rodríguez, B.E. Quevedo-Hidalgo, Impact of antibiotics as waste, physical, chemical, and enzymatic degradation: use of laccases, *Molecules* 27 (2022) 4436.
- [5] S. Ren, S. Wang, Y. Liu, Y. Wang, F. Gao, Y. Dai, A review on current pollution and removal methods of tetracycline in soil, *Sep. Sci. Technol.* 58 (2023) 2578–2602.
- [6] T. Liu, C.O. Aniagor, M.I. Ejimofor, M.C. Menkiti, K.H.D. Tang, B.L.F. Chin, Y. H. Chan, C.L. Yiin, K.W. Cheah, Y.H. Chai, Technologies for removing pharmaceuticals and personal care products (PPCPs) from aqueous solutions: recent advances, performances, challenges and recommendations for improvements, *J. Mol. Liq.* 374 (2023) 121144.
- [7] S.F. Chua, A. Nouri, W.L. Ang, E. Mahmoudi, A.W. Mohammad, A. Benamor, M. Ba-Abbad, The emergence of multifunctional adsorbents and their role in environmental remediation, *J. Environ. Chem. Eng.* 9 (2021) 104793.
- [8] F. da Silva Bruckmann, C.E. Schnorr, T. da Rosa Salles, F.B. Nunes, L. Baumann, E. I. Müller, L.F.O. Silva, G.L. Dotto, C.R. Bohn Rhoden, Highly efficient adsorption of tetracycline using chitosan-based magnetic adsorbent, *Polymers* 14 (2022) 4854.
- [9] X. Liu, Z. Shao, Y. Wang, Y. Liu, S. Wang, F. Gao, Y. Dai, New use for *Lentinus edodes* bran biochar for tetracycline removal, *Environ. Res.* 216 (2023) 114651.
- [10] M. Aliyu, A.H. Abdullah, M.I. bin, Mohamed Tahir, Adsorption tetracycline from aqueous solution using a novel polymeric adsorbent derived from the rubber waste, *J. Taiwan Inst. Chem. Eng.* 136 (2022) 104333.
- [11] T. Wang, L. Xue, Y. Liu, L. Zhang, B. Xing, N self-doped hierarchically porous carbon derived from biomass as an efficient adsorbent for the removal of tetracycline antibiotics, *Sci. Total Environ.* 822 (2022) 153567.
- [12] T.M.P. Nguyen, H.T. Van, M. Yilmaz, T.K. Hoang, Q.T. Nguyen, T.M.H. Vi, L.T. Q. Nga, Removal of Tetracycline from aqueous solution using composite adsorbent of ZnAl layered double hydroxide and bagasse biochar, *Environ. Technol. Innov.* 28 (2022) 102914.
- [13] Q. Shi, W. Wang, H. Zhang, H. Bai, K. Liu, J. Zhang, Z. Li, W. Zhu, Porous biochar derived from walnut shell as an efficient adsorbent for tetracycline removal, *Bioresour. Technol.* 383 (2023) 129213.
- [14] H. Sereshiti, E. Beyrak-Abadi, M. Esmaili Bidhendi, I. Ahmad, S. Shahabuddin, H. Rashidi Nodeh, N. Sridevi, W.N. Wan Ibrahim, Sulfide-Doped magnetic carbon nanotubes developed as adsorbent for uptake of tetracycline and cefixime from wastewater, *Nanomaterials* 12 (2022) 3576.
- [15] C. Hu, J. Jiang, Y. Li, Y. Wu, J. Ma, H. Li, H. Zheng, Eco-friendly poly (dopamine)-modified glass microspheres as a novel self-floating adsorbent for enhanced adsorption of tetracycline, *Sep. Purif. Technol.* 292 (2022) 121046.
- [16] H. Jiang, Y. Dai, Vitamin C modified crayfish shells biochar efficiently remove tetracycline from water: a good medicine for water restoration, *Chemosphere* 311 (2023) 136884.
- [17] Z. Çiğeroğlu, E.S. Kazan-Kaya, N. El Messaoudi, Y. Fernine, J.H.P. Américo-Pinheiro, A. Jada, Remediation of tetracycline from aqueous solution through adsorption on g-C₃N₄-ZnO-BaTiO₃ nanocomposite: optimization, modeling, and theoretical calculation, *J. Mol. Liq.* 369 (2023) 120866.
- [18] M.R. Awual, M.M. Hasan, M.A. Khaleque, M.C. Sheikh, Treatment of copper (II) containing wastewater by a newly developed ligand based facial conjugate materials, *Chem. Eng. J.* 288 (2016) 368–376.
- [19] M.E. Awual, M.S. Salman, M.M. Hasan, M.N. Hasan, K.T. Kubra, M.C. Sheikh, A. I. Rasee, A.I. Rehan, R.M. Waliullah, M.S. Hossain, Ligand imprinted composite adsorbent for effective Ni (II) ion monitoring and removal from contaminated water, *J. Ind. Eng. Chem.* 131 (2024) 585–592.
- [20] M.R. Awual, M.M. Hasan, H. Znad, Organic-inorganic based nano-conjugate adsorbent for selective palladium (II) detection, separation and recovery, *Chem. Eng. J.* 259 (2015) 611–619.
- [21] S.S. Priya, K.V. Radha, A review on the adsorption studies of tetracycline onto various types of adsorbents, *Chem. Eng. Commun.* 204 (2017) 821–839.
- [22] S.H. Mosavi Mirak, S. Sharifian, F.Esmaili Khalil Saraei, N. Asasian-Kolur, B. Haddadi, C. Jordan, M. Harasek, Titanium-Pillared clay: preparation optimization, characterization, and artificial neural network modeling, *Materials (Basel)* 15 (2022) 4502.
- [23] H. Najafi, S. Farajfaed, S. Zolgharnian, S.H.M. Mirak, N. Asasian-Kolur, S. Sharifian, A comprehensive study on modified-pillared clays as an adsorbent in wastewater treatment processes, *Process Saf. Environ. Prot.* 147 (2021) 8–36.
- [24] P. Yuan, H. He, F. Bergaya, D. Wu, Q. Zhou, J. Zhu, Synthesis and characterization of delaminated iron-pillared clay with meso-microporous structure, *Microporous Mesoporous Mater.* 88 (2006) 8–15.
- [25] H. Najafi, N. Asasian-Kolur, S. Sharifian, Adsorption of chromium (VI) and crystal violet onto granular biopolymer-silica pillared clay composites from aqueous solutions, *J. Mol. Liq.* 344 (2021) 117822.
- [26] B. Chekmane, F. Zermane, M. Baudu, O. Bouras, J.P. Basly, Sorption of basic dyes onto granulated pillared clays: thermodynamic and kinetic studies, *J. Colloid Interface Sci.* 381 (2012) 158–163.
- [27] B. Chekmane, O. Bouras, M. Baudu, J.P. Basly, A. Cherguelaine, Granular inorgano-organo pillared clays (GIOCs): preparation by wet granulation, characterization and application to the removal of a Basic dye (BY28) from aqueous solutions, *Chem. Eng. J.* 158 (2010) 528–534.
- [28] A. Louadj, O. Bouras, B. Chekmane, F. Zermane, Synthesis of new granular surfactant iron pillared montmorillonite with gluten: application to the removal of cationic dyes in mixture systems, *Desalination Water Treat.* 98 (2017) 315–325.
- [29] S. Sharifian, N. Asasian-Kolur, H. Najafi, B. Haddadi, C. Jordan, M. Harasek, Reusable granulated silica pillared clay for wastewater treatment, selective for adsorption of Ni (II), *Clean Eng Technol* 14 (2023) 100634.
- [30] S. Farajfaed, S. Sharifian, N. Asasian-Kolur, M. Sillanpää, Granular silica pillared clay for levofloxacin and gemifloxacin adsorption from aqueous systems, *J. Environ. Chem. Eng.* 9 (2021) 106306.
- [31] D.C.M. Ferreira, T.C. Dos Santos, J.S. dos Reis Coimbra, E.B. de Oliveira, Chitosan/carboxymethylcellulose polyelectrolyte complexes (PECs) are an effective material for dye and heavy metal adsorption from water, *Carbohydr. Polym.* 315 (2023) 120977.
- [32] A.I. Abd-Elhamid, E.M. Abu Elgoud, H.F. Aly, Graphene oxide modified with carboxymethyl cellulose for high adsorption capacities towards Nd (III) and Ce (III) from aqueous solutions, *Cellulose* 29 (2022) 9831–9846.
- [33] S. Xia, X. Xu, C. Xu, Y. Zheng, G. Liu, Synthesis and characterization of magnetic cmC-CoFe₂O₄ adsorbents in removing and recovering phosphate, *Fresenius Environ. Bull.* 24 (2015) 1025–1031.
- [34] J. Wang, X. Lin, X. Luo, W. Yao, Preparation and characterization of the linked lanthanum carboxymethylcellulose microsphere adsorbent for removal of fluoride from aqueous solutions, *RSC Adv.* 5 (2015) 59273–59285.
- [35] M. Thommes, K. Kaneko, A. Neimark, J. Olivier, F. Rodriguez-Reinoso, J. Rouquerol, K. Sing, Physisorption of gases, with special reference to the evaluation of surface area and pore size distribution (IUPAC Technical Report), *Pure Appl. Chem.* 87 (2015), <https://doi.org/10.1515/pac-2014-1117>.
- [36] L.F. Isernia, TIR study of the relation, between extra-framework aluminum species and the adsorbed molecular water, and its effect on the acidity in ZSM-5 steamed zeolite, *Mater. Res.* 16 (2013) 792–802.
- [37] J. Madejová, M. Pentrák, H. Pálková, P. Komadel, Near-infrared spectroscopy: a powerful tool in studies of acid-treated clay minerals, *Vib. Spectrosc.* 49 (2009) 211–218.
- [38] M.N. Chai, M.I.N. Isa, The oleic acid composition effect on the carboxymethyl cellulose based biopolymer electrolyte, *Journal of Crystallization Process and Technology* 3 (2013) 1–4.
- [39] H.N. Bhatti, S. Sadaf, M. Iqbal, Y. Safa, H. Ain, S. Nawaz, A. Nazir, Enhanced adsorption of Foron Black RD 3GRN dye onto sugarcane bagasse biomass and Na-alginate composite, *Desalination Water Treat.* 216 (2021) 423–435, <https://doi.org/10.5004/dwt.2021.26893>.
- [40] P.J. Launer, B. Arkles, Infrared analysis of organosilicon compounds: structure correlations, *Silicone Compounds Register Review* 100 (1987) 100–103.
- [41] S.J. Parikh, K.W. Goyne, A.J. Margenot, F.N.D. Mukome, F.J. Calderón, Soil chemical insights provided through vibrational spectroscopy, *Adv. Agronomy* 126 (2014) 1–148.
- [42] G.C. Fard, M. Mirjalili, F. Najafi, Preparation of nano-cellulose/A-Fe₂O₃ hybrid nanofiber for the cationic dyes removal: optimization characterization, kinetic, isotherm and error analysis, *Red* 46 (2018) 401–403.
- [43] P. Cambier, Infrared study of goethites of varying crystallinity and particle size: I. Interpretation of OH and lattice vibration frequencies, *Clay Miner.* 21 (1986) 191–200.
- [44] J. Ning, P. Shi, M. Jiang, C. Liu, X. Li, Effect of Ce doping on the structure and chemical stability of nano- α -Fe₂O₃, *Nanomaterials* 9 (2019) 1039.
- [45] B.B. Zviagina, V.A. Drits, O.V. Dorzhieva, Distinguishing Features and Identification Criteria for K-Dioctahedral 1M Micaceous (Illite-Aluminoceladonite and Illite-Glaucanite-Celadonite Series) from Middle-Infrared Spectroscopy Data, *Minerals* 10 (2020) 153.
- [46] J. Reijenga, A. Van Hoof, A. Van Loon, B. Teunissen, Development of methods for the determination of pKa values, *Anal. Chem. Insights* 8 (2013) S12304. ACI-.
- [47] S. Lagergren, Zur theorie der sogenannten adsorption gelöster stoffe, *Kungliga Svenska Vetenskapsakademiens Handlingar* 24 (1898) 1–39.
- [48] Y.S. Ho, G. McKay, The kinetics of sorption of divalent metal ions onto sphagnum moss peat, *Water Res.* 34 (2000) 735–742.
- [49] W.J. Weber Jr, J.C. Morris, Kinetics of adsorption on carbon from solution, *J. Sanitary Eng. Division* 89 (1963) 31–59.

- [50] Q. Song, Y. Fang, Z. Liu, L. Li, Y. Wang, J. Liang, Y. Huang, J. Lin, L. Hu, J. Zhang, The performance of porous hexagonal BN in high adsorption capacity towards antibiotics pollutants from aqueous solution, *Chem. Eng. J.* 325 (2017) 71–79.
- [51] T. Chen, T. Da, Y. Ma, Reasonable calculation of the thermodynamic parameters from adsorption equilibrium constant, *J. Mol. Liq.* 322 (2021) 114980.
- [52] P. Saha, S. Chowdhury, Insight into adsorption thermodynamics, *Thermodynamics* 16 (2011) 349–364.
- [53] M.K. Trivedi, S. Patil, H. Shettigar, K. Bairwa, S. Jana, K. Bairwa, Spectroscopic characterization of chloramphenicol and tetracycline: an impact of biofield, *Pharm. Anal. Acta* 6 (2015) 19–21.
- [54] D. Predoi, S.L. Iconaru, M.V. Predoi, N. Buton, Development of novel tetracycline and ciprofloxacin loaded silver doped hydroxyapatite suspensions for biomedical applications, *Antibiotics* 12 (2022) 74.
- [55] C.M. Lawrence, *Organic Chemistry I Drill (CHEM2210D)-Module 2-Functional Groups and Infrared Spectroscopy, Course Modules 8* (2019). https://digitalcommons.xula.edu/doc_cm (accessed February 16, 2024).
- [56] H. Guo, B. Niu, X. Wu, Y. Zhang, S. Ying, Effective removal of 2, 4, 6-trinitrophenol over hexagonal metal-organic framework NH₂-MIL-88B (Fe), *Appl. Organomet. Chem.* 33 (2019) e4580.
- [57] M.R. Awual, M.N. Hasan, M.M. Hasan, M.S. Salman, M.C. Sheikh, K.T. Kubra, M. S. Islam, H.M. Marwani, A. Islam, M.A. Khaleque, Green and robust adsorption and recovery of Europium (III) with a mechanism using hybrid donor conjugate materials, *Sep. Purif. Technol.* 319 (2023) 124088.
- [58] M.S. Salman, M.C. Sheikh, M.M. Hasan, M.N. Hasan, K.T. Kubra, A.I. Rehan, M. E. Awual, A.I. Rasee, R.M. Waliullah, M.S. Hossain, Chitosan-coated cotton fiber composite for efficient toxic dye encapsulation from aqueous media, *Appl. Surf. Sci.* 622 (2023) 157008.
- [59] A.I. Rehan, A.I. Rasee, M.E. Awual, R.M. Waliullah, M.S. Hossain, K.T. Kubra, M. S. Salman, M.M. Hasan, M.N. Hasan, M.C. Sheikh, Improving toxic dye removal and remediation using novel nanocomposite fibrous adsorbent, *Colloids Surf A Physicochem Eng Asp* (2023) 131859.